Chaperone-Like Activity of Human Small Heat Shock Protein-Derived Peptides in Response to Cellular Stress

By

Emily Gliniewicz

Thesis Advisor: Kathryn McMenimen

A Paper Presented to the

Faculty of Mount Holyoke College in

Partial Fulfillment of the Requirements for

The Degree of Bachelor of Arts

with Honor

Department of Biochemistry

South Hadley, MA 01075

May 2019

ACKNOWLEDGEMENTS

To Katie McMenimen, thank you for always being a source of encouragement, an open door, a listening ear. I value having had so much time with you as my mentor, beginning my first spring here at Mount Holyoke. You have reminded me that relaxing and having fun are important uses of time, and that perfection isn't always necessary. You have taught me that thinking ahead is valuable, both in science and beyond, and that mistakes aren't the end of the world.

To Elizabeth De Leon, thank you for being such an enthusiastic, patient, and knowledgeable teacher. You taught me the basics of lab techniques and how to problem solve and think independently in research. I am forever grateful for your mentorship and positive influence on my career in science.

To Katie Berry, thank you for being so devoted to my understanding of biochemistry. I cherish every early Friday morning in your office drinking our coffee and going over my notes. You make biochemistry fun, and you showed me how worthy of our appreciation are all aspects of life so small we cannot see. Your passion and curiosity are infectious, and you have inspired me to get excited about creating research questions and trying to find answers.

And to Cheri Bickford and Mark Gliniewicz, my parents, thank you for preparing for 18 years to be able to give me this opportunity. Thank you for being proud of every achievement, no matter how small. Thank you for the phone calls, the words of encouragement, the hugs, the pats on the back. Thank you for all the miles driven, all the boxes carried up many flights of stairs, and the steady supply of comfort food. I haven't forgotten for a moment that you're always there when I turn around.

TABLE OF CONTENTS

LIST OF FIGURES AND TABLES

ABSTRACT

Small heat shock proteins (sHsps), a family of molecular chaperones that prevent aggregation of partially unfolded protein substrates, are present in many different organisms across all domains of life. They work to maintain cellular function and survival under stress conditions, such as high temperatures, by binding non-natively folded proteins in an ATP-independent manner. This is followed by either promotion of proper protein folding or facilitation of protein degradation. Malfunction of sHsps in humans has been implicated in the development of several morbidities, particularly in neurological diseases where accumulation of misfolded proteins leads to neurodegeneration. sHsps contain an "alpha-crystallin domain" (ACD) flanked by an N- and C-terminal region (NTR and CTR, respectively) of varying length and sequence. These terminal regions are believed to participate in substrate and quaternary interactions. Their quaternary interactions result in the formation of dynamic oligomers whose physiological relevance and role in chaperone activity has yet to be determined.

This work includes two projects, both with aims to identify functional regions of sHsps that contain chaperone activity. In the first, purifying the relatively unstructured N-terminal sequence from human HspB1 and analyzing its interaction with model substrates, we have identified an 88-residue sequence that exhibits chaperone activity in solution. We constructed gold nanoparticles (AuNPs) conjugated to the HspB1 NTR to explore the importance of the oligomeric interactions of the molecular chaperone in binding to its substrate. These sHsp-AuNPs were found to exhibit chaperone activity, with the chaperone capacity varying by substrate and AuNP diameter. Our combined results indicate the particular importance of the NTR in sHsp chaperone activity and demonstrate the therapeutic potential of sHsp-AuNPs.

The second project evaluated the chaperone-like activity of mini alpha-Crystallin A (CryAAID1), residues 70-88 of human sHsp alpha-Crystallin A. This peptide was also conjugated to AuNPs and results confirmed CryAAID1 maintained chaperone activity in the absence of other sHsp domains. Substrate specificity AuNP diameter dependence were also demonstrated.

CHAPTER 1 | INTRODUCTION

1.1 | Protein Conformational Disorders

Conformational disorders include neurodegenerative diseases like Alzheimer's Disease (AD) and Parkinson's Disease (PD), which result from changes in protein conformation, leading to aggregation and a decline in cell health or death.[1] AD and PD are the two most common known diseases of their kind.[2] Mechanisms exist in healthy cells to sequester toxic aggregates and clear them from the cell, though these mechanisms have the potential to go awry during the onset of a neurodegenerative disease. Protein aggregates build up inside and outside of cells in the brain leading to varying pathologies.[1] Gaining a molecular understanding of these conformational diseases, beginning with their biological and biochemical basis, is important for developing means of early diagnosis and preventative treatments, since the earlier medical intervention can occur, the less irreversible memory loss is experienced by the patient.[1] Future successful treatments may stop toxic aggregates from forming, alleviate environmental stressors that cause or accelerate aggregation, or may instead accelerate the degradation and removal of these aggregates.[1,2] Elderly patients are often affected by more than one neurodegenerative disease. For instance, a large proportion of patients with PD also exhibit AD-related pathology and vice versa.[3]

AD occurs gradually, beginning with mild cognitive impairment (MCI), which presents as mild disturbances of memory and difficulty performing

demanding cognitive tasks.[1] Patients live, on average, eight years after the onset of symptoms.[1] A decline in memory and cognition progresses as the disease advances.[1] AD begins to involve personality and behavior changes, then loss of speech and movement in later stages. The later stages of AD ultimately lead to total disability and death given there is no known cure at this time.[1] Today's treatments aim to slow the progression of the disease and provide relief from the symptoms.[1]

The predominant pathology of AD is the misfolding and aggregation of the proteins amyloid-beta (Aβ) and tau (Figure 1).[2] Aβ and tau are classified as intrinsically disordered proteins (IDPs) due to their ability to adopt a range of different structures, allowing them to perform a variety of functions within the cell.[2] Experimental data shows a negative correlation between the concentrations of soluble (unaggregated) Aβ and tau proteins with cognitive decline in both AD animal models and human patients.[2] There is a possibility cerebrospinal fluid testing could be used as a diagnostic tool to compare current and baseline levels of Aβ and tau in patients with AD. However, this tool is not ideal due to the pain and lengthiness of the test.[1] Presently, AD can only be diagnosed conclusively post-mortem, although neuroimaging allows visualization of amyloid plaques and neurofibrillary tangles in the brains of live patients, suggesting the presence of the disease.[1] Potential treatment development is considering molecular machines to break up aggresomes, or perhaps vaccinating against amyloid plaques so the body will destroy them.[1]

There are two abnormal structures found in the brain of an AD patient.[1] The first, amyloid plaques, are deposits of the Aβ protein and are located extracellularly (Figure 1).[1] Amyloid plaques have high beta-sheet (secondary protein structure discussed in the following section) content, lending to their fibrous character.[2] Misfolded Aβ forms toxic oligomers (assemblies of misfolded, soluble protein) in a range of sizes.[1,2] The high concentration of beta-sheets within these oligomers is largely responsible for their toxic pathology.[2] Early stage oligomers are considered aggregation intermediates and may be involved in the spreading and advancement of AD within the patient.[2] Addition of Aβ monomers (single protein units) to soluble growing oligomers creates insoluble fibrils, which are then considered aggregates.[2] Aggregates are then sequestered into an "aggresome" within the cell, a structure whose function remains unknown.[1] Inherited mutations on the gene encoding the amyloid precursor protein have been found to increase aggregation of Aβ.[1]

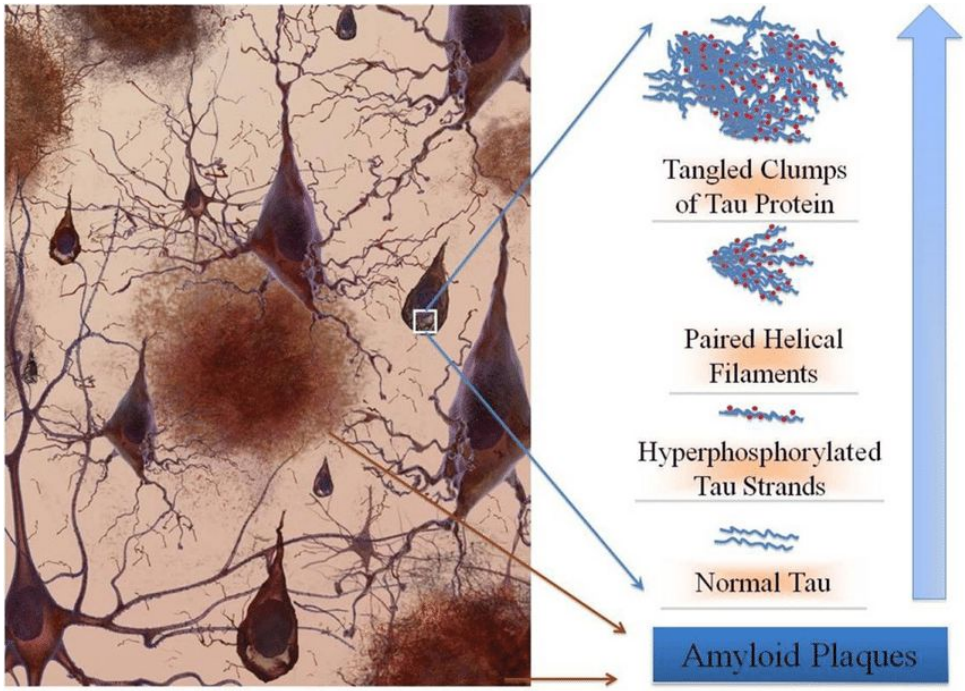

Figure 1. Overview of aggregates in Alzheimer's Disease. Alzheimer's disease is associated with aggregates of the proteins amyloid-beta and tau, which form plaques and tangles, respectively. These aggregates are present within and around neurons, damaging nervous system functions. Adapted from Ahlschwede *et al*., 2012.[4]

The second abnormal structure associated with AD is the neurofibrillary tangle. Neurofibrillary tangles are helical filaments made of hyperphosphorylated tau protein and are found intracellularly (Figure 1).[1] Tau is a microtubule-associated protein that can be transmitted from cell to cell to spread its pathology throughout the brain.[5] This protein plays a role in the assembly and stabilization of microtubules and is essential for intracellular transport within neurons.[5] The involvement of tau in AD characterizes AD as a tauopathy.[5] Tau has been shown to have distinct folds for each of the known tauopathies, supported by the

identification of 18 different tau strains.[5] Tau's mechanism of propagation is still disputed. Mechanisms to consider include synaptic transmission, microglia-mediated propagation, and transmission via extracellular vesicles.[5] Evidence suggests oligomeric forms of tau may disrupt microtubule stability and trafficking, and also cause mitochondrial dysfunction by decreasing the activity of complex I in the electron transport chain (ETC).[2] Hyperphosphorylation of tau leads to a conformational change in tau itself, as well as microtubule disassembly, and eventually aggregation reaches the point of neurofibrillary tangle formation.[5]

Questions involving causes of AD still remain largely unanswered.[1] Several hypotheses exist, such as that of increased concentration of metal ions in the brain promoting protein aggregation. Abnormal metabolism of metal ions can lead to the production of reactive oxygen species (ROS), the presence of which further damages proteins and causes more extensive aggregation.[1,2] A similar hypothesis relating to ROS is being considered for the development of other neurodegenerative diseases, such as PD.

PD is associated with the accumulation of alpha-synuclein deposits and is therefore considered a synucleinopathy.[5] Its primary pathology is the misfolding and aggregation of the alpha-synuclein protein.[2] Like AD, PD is a progressive degenerative disease of the human nervous system.[3] One of the main challenges in preventing or treating PD is that its symptoms manifest only after the disease has advanced significantly.[3] The disease is usually diagnosed with

the appearance of the first motor symptoms: slowness of initiation of voluntary movements, reduction in speed of repetitive actions, muscular rigidity, resting tremor, postural instability, and gait disturbances like shuffling.[6] There also exists a possibility for speech disturbances and problems swallowing.[6] Pre-motor symptoms may start as early as 10 years prior to diagnosis and include a lack of emotional involvement and interest, excessive daytime sleepiness, mood disturbances, loss of taste and smell, and sleep disturbances.[6]

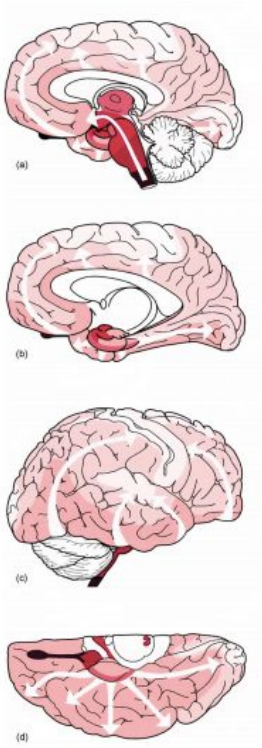

Figure 2. Staging the spreading of Parkinson's Disease. Parkinson's Disease is a progressive degenerative disease of the human nervous system, often diagnosed at the first appearance of motor symptoms. Its pathological stages are identified by the regions of the brain they affect. The presymptomatic stage is confined to the medulla oblongata and olfactory bulb. As the disease progresses, symptoms begin to involve the mid- and forebrain. End-stage symptoms display severe involvement of the brain and a wide variety of clinical manifestations. Adapted from Braak *et al*., 2003.[3]

PD has been divided into six pathological stages. The presymptomatic phase of PD is made up of stages one and two, during which inclusion bodies are confined to the medulla oblongata and olfactory bulb (Figure 2).[3,6] Appearance of inclusion bodies is a definitive sign of disease, since these structures are not considered part of normal brain aging.[3] Stages three and four mark the development of clinical symptoms and the involvement of the mid- and forebrain (Figure 2).[6] End-stage PD consists of stages five and six, where inclusion bodies have entered the neocortex, there is severe involvement of the brain, and a wide variety of clinical manifestations.[3,6] Most clinical symptoms of PD involve motor disturbances, as described above, which are caused by the degeneration of dopaminergic neurons.[6] As is true for AD, there is currently no available treatment that will halt the progression of PD or reverse any damage.[6] Existing treatments aim to correct motor disturbances. Some of these treatments have a good response early on, but then display "wearing-off" symptoms, followed by "on-off" symptoms as PD progresses.[6] These medications have also been reported to cause hallucinations, as well as psychosis, late in the disease at high doses.[6]

The inclusion bodies specific to PD are formed from the aggregation of alpha-synuclein.[3] Two forms of alpha-synuclein inclusion bodies have been discovered post-mortem in the brains of patients who had PD: Lewy bodies (LBs) and Lewy neurites (LNs). LBs are proteinaceous and spherical, sharing many of

the same characteristics as aggresomes found in AD.[1,6] LNs are thread-like, branching forms of aggregated alpha-synuclein.[6] Interestingly, within the structure of alpha-synuclein, the central region is particularly aggregation-prone (Figure 3).[6] The N- and C- terminal regions of the protein have been shown to interact with one another, perhaps to protect the central region from aggregation, as is supported by evidence that alpha-synuclein truncated at the C-terminus aggregates much faster than the full-length protein (Figure 3).[6] Mutations of the gene coding for alpha-synuclein have been linked to onset of PD.[5] Alpha-synuclein, like tau in AD, can be transmitted from cell to cell, acting as a seed for aggregation and initiating the spread of the pathology.[6] Evidence suggests alpha-synuclein aggregates can be released from neurons and taken up by astroglial cells, triggering an inflammatory response.[2] Alpha-synuclein is highly conserved among vertebrate species, which

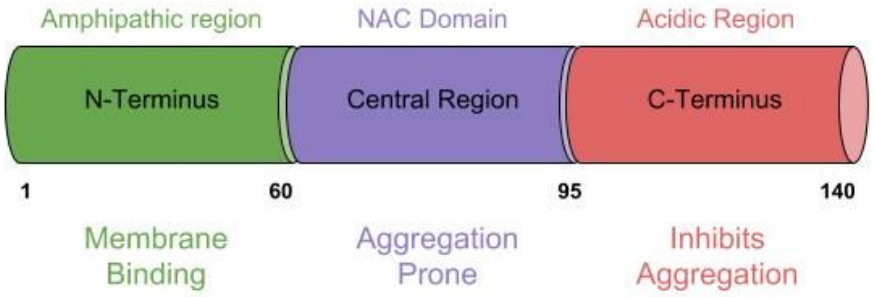

Figure 3. Sequence diagram of alpha-synuclein. Parkinson's Disease is associated with the formation of inclusion bodies, which are aggregates of the protein alpha-synuclein. The central region of alpha-synuclein is particularly aggregation-prone, while both the N- and C-terminalregions have been shown to protect the central region from aggregation.[5]

suggests its physiological role is a vital one.[5] Like Aβ in AD, alpha-synuclein is part of a family of IDPs.[6] Its native disordered structure enables it to demonstrate "conformational plasticity" and accommodate different substrates depending on their primary amino acid sequences.[6] Alpha-synuclein is abundant at the presynaptic terminal of neurons, and it remains unclear why it leaves the synaptic terminal and transforms into insoluble LBs and LNs.[3,5] Alpha-synuclein has also been found in mitochondria, endoplasmic reticula, and nuclei.[5] It interacts with other proteins, lipids, and components of the cytoskeletal matrix, modulating protein trafficking and maintaining synaptic homeostasis.[5] Like tau in AD, there's evidence that alpha-synuclein aggregates also cause mitochondrial dysfunction, involving both complex I of the

ETC and the outer mitochondrial membrane and its transport of proteins.[2]

1.2 | Protein Structure and Folding

I. Translation and Protein Conformation

The preinitiation complex of translation consists of the two ribosomal subunits associated with several nonribosomal proteins, many eukaryotic initiation factors, a tRNA charged with methionine, and finally, the mRNA to be translated.[7] Initiation factors are proteins of various sizes that cycle on and off ribosomes during translation. They perform functions such as helping to identify the start codon and appropriate tRNA binding sites on the ribosome, as well as correctly positioning the mRNA for the scanning process.[8] Evidence suggests regulation of protein synthesis by these initiation factors is tissue-specific. Although the same translation factors may be present in all cells, their relative expression levels may differ between cell types.[8] Whenthe initiator tRNA recognizes the start codon, scanning slows and stalls, and the initiator tRNA participates in the synthesis of the first peptide bond of the protein being synthesized.[8]

The Met-charged initiator tRNA binds to one of three binding sites on the ribosome, the P site.[7] All other codons to be translated meet their respective tRNAs in the site on the ribosome adjacent to the P site, called the A site.[7] A series of elongation reactions on the ribosome are repeated as each codon is

translated into an amino acid and added to the growing polypeptide chain.[7] The translocation of the ribosome along the mRNA during these elongation reactions is aided by elongation factors and the hydrolysis of GTP.[8] After an amino acid is added to the growing chain, the peptidyl-tRNA that has just received the polypeptide chain is switched to the P site and the deacylated tRNA is transferred to the ribosome's third binding site, the E site.[8] This series of transfers leaves the A site open for the next charged tRNA to meet its match.[7] When a termination codon is brought into the A site, a release factor (RF) binds to terminate translation; the completed polypeptide is released and the complex disassembles.[7,8] The nascent polypeptide chain then undergoes considerable posttranslational modifications, which often lead to more than one active protein product.[7]

In addition to any modifications to the linear chain of amino acids, the polypeptide must fold into a unique three-dimensional structure in order to carry out its cellular function.[7] Protein folding is hierarchical, including a primary, secondary, tertiary, and sometimes even quaternary level of folding complexity.[9] Protein folding is largely dependent on the cellular environment and is highly error-prone.[7,9] If folding mistakes occur, some proteins are able to spontaneously refold.[9] However, some misfolded proteins, especially those with exposed hydrophobic residues, are unable to refold, and begin to accumulate, forming toxic aggregates within the cell.[7] To prevent misfolding,

cells express a class of proteins called chaperones that receive nascent proteins directly from the ribosome and guide them along the correct folding pathway to their native three-dimensional structure.[7]

Protein folding refers to the process where the polypeptide chain rearranges to acquire its native structure.[10] A protein's native structure is one that gives the macromolecule the lowest possible Gibbs free energy.[9] In aqueous environments, this is usually accomplished by burying hydrophobic groups in the core of the protein.[9] Not all polypeptides need the assistance of chaperones to reach their native fold, but regardless of independence, protein folding is accomplished within just seconds or minutes.[10] Often, large multi-domain proteins begin folding early, while still on the ribosome.[10] This is called cotranslational folding.[10] Despite an early start, the protein still will not reach its complete native structure until its translation is complete.[10] While the growing polypeptide chain is still on the ribosome, co-translational folding commonly accomplishes the formation of alpha helices or small tertiary structural elements.[7] The exit channel of the ribosome seems to mimic the interior of a chaperone protein, and may influence folding in a similar way.[7]

A protein's primary structure consists of the polypeptide backbone: a linear series of planar *trans* peptide bonds and the side chains of the corresponding amino acids.[9] The bond angles within the backbone are highly dependent on the identity of the specific residues.[9] Common secondary structures

include alpha-helices, beta-sheets, and turns.[9] The formation of an alpha-helix largely relies on hydrogen bonding networks.[9] The helix can be right- or left-handed (with right-handed being most stable) and can differ in the number of amino acids per turn of the helix, as well as the number of amino acids within the helix that are participating in hydrogen bonds.[9] Beta-sheets can be parallel or antiparallel, with the differences between the two arrangements being the hydrogen bond formations and amino acid composition (Figure 4).[9]

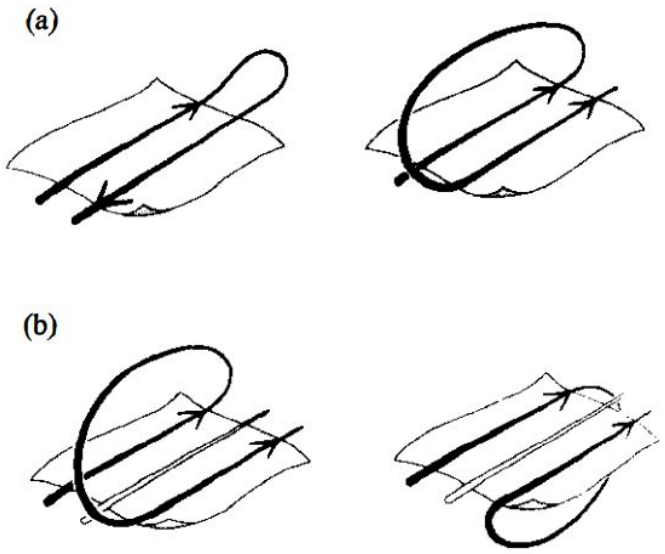

Figure 4. Topological connections in beta sheets. Beta sheets are one of the major secondary structures in protein folding. Beta sheets can be parallel or antiparallel depending on the arrangements of hydrogen bonds between strands. Both parallel and antiparallel forms can be connected in several ways. **(a)** Left is a hairpin connection, right is a single cross-over. **(b)** Left is a right-handed double cross-over connection, right is a left-handed double cross-over. Adapted from Rossmann, 1981.[9]

Sharp turns connect different secondary structural elements, and take different forms based on amino acid composition.[9] Turns are particularly frequent

in globular proteins.[9] They have four amino acids connected by three peptide bonds, and are stabilized by a single hydrogen bond between the first and forth residues.[9] Glycine (Gly) is a particularly favorable residue for turns because of its lack of steric hindrance.[9] Super-secondary structure is the packing of simpler secondary structures into a clear tertiary formation, likely because of the energetic stability of such a structure.[9]

An example of a super-secondary structure is the pattern beta-alpha-beta.[9] Such a series of secondary structures forms what's considered a functional domain.[9] There can be multiple domains within a protein, each folding independently, then coming together to form the protein's tertiary structure.[9] Folding into tertiary structure relies on many weak, noncovalent interactions between amino acids both close in primary sequence and further apart.[7] These domains are spatially separated from one another within the polypeptide and often each have a distinct function.[9] A protein's final tertiary structure can sometimes be the repeat of a single domain several times along the same polypeptide chain.[9] Finally, there's quaternary structure, which does not exist in all proteins, but consists of the coming together of separate subunits. Quaternary structure is often responsible for the functional regulation of multiple subunits in an enzyme or protein complex.[9]

In order to reach their native folds, proteins must pass through a series of folding intermediates, represented by folding funnel diagrams: models used to explain the rapid path a protein takes to reach its final structure (Figure 5).[10] There

are an almost infinite number of possible structures a single polypeptide chain can form, all of which differ in stability, represented by Gibbs free energy.[10] The native and misfolded states of a protein are separated by a high barrier of this free energy, and the height of this barrier determines the rate of the protein's transition from folded to misfolded (Figure 5).[10] The high barrier and low Gibbs free energy of aggregates contribute to the difficult reversal of aggregation.

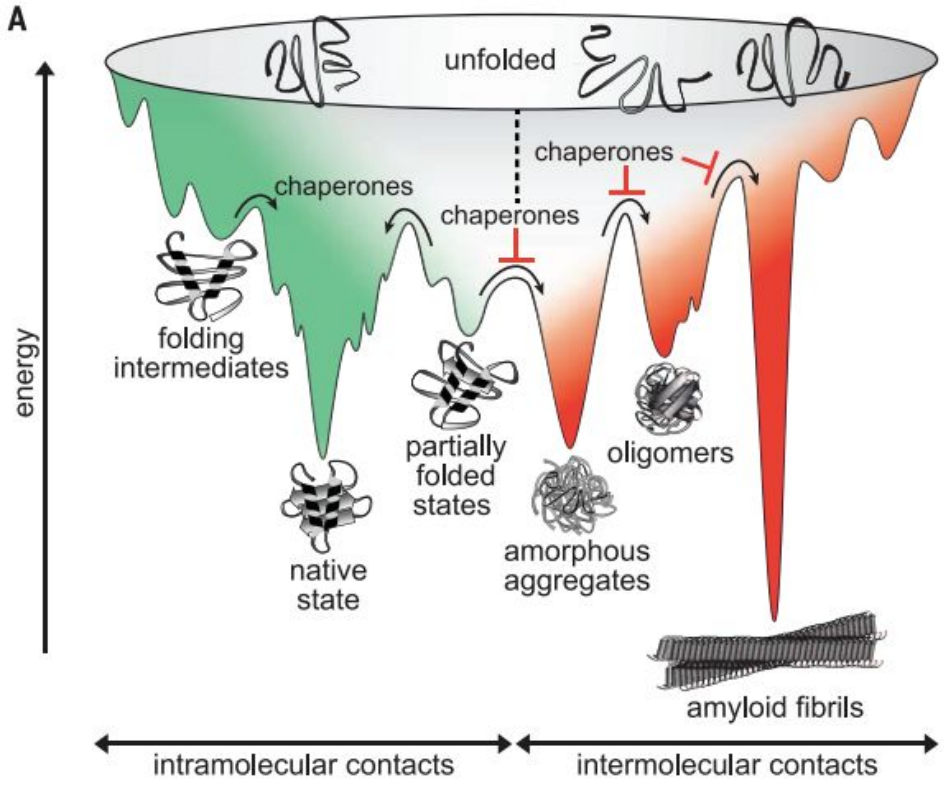

Figure 5. Folding funnel diagrams explain protein folding pathways. In order to reach their native folds, proteins pass through several intermediate structures. Folding funnels are models used to explain the energy differences among structures that guide a protein to its native, low energy, functional state. These diagrams also show the high energies required to escape an aggregate state, and the inhibiting of the entrance of aggregated states by chaperones. Adapted from Balchin *et al*., 2016.[7]

For water soluble proteins, hydrophobic forces are particularly relevant in driving the collapse and burial of nonpolar amino acids within the core of the folding structure of soluble proteins. Charged residues are usually exposed on the protein's surface. Favorable pairing between two nonpolar residues and electrostatic interactions between two oppositely charged residues contribute significantly to the stability of tertiary structure.[11] Functional roles of the protein as an enzyme have a strong impact on the spatial placement of charged residues within its native structure, since particular charged residues are likely involved in the catalysis themselves.[11] Because pH affects the protonation states of charged residues, protein folding is strongly dependent on the pHof the environment.[11] All of the forces mentioned above contribute to the decrease in conformational space that must be searched during the folding process.[7] The "energy funnel" directs the protein down a path toward obtaining its lowest energy structure.[10] Proteins do *not* test out every possible structure on their way to that of the lowest energy because that could take *years* . The "energy funnel" starts working at the level of secondary structures, which are largely determined by local amino acid sequences.[10] The main support for such a model is its ability to accelerate the rate of protein folding by a significant number of orders of magnitude. Determining the three-dimensional structure of a protein or protein complex is important for

understanding mechanisms of action and for determining how dysregulated systems can malfunction.

II. Methods for Understanding Protein Structure

Fluorescence and Fluorescent Dyes

The excitation and subsequent emission of light by electrons of dye molecules leads to the production of fluorescence. This exchange from ground state, S_0, to excited state happens within femtoseconds.[11] The relaxation of the donor atom back to S_0 is responsible for fluorescence emission.[12] Fluorescence spectroscopy is a highly sensitive method for analyzing the structure and function of various proteins.[12]

Noncovalently-attached, extrinsic fluorescent dyes are used to study proteins in various ways.[12] They're capable of characterizing the folding process of a protein, including its intermediates, measuring a protein's surface hydrophobicity, or detecting its aggregation.[12] Noncovalent dye-protein interactions are predominantly hydrophobic and electrostatic in nature. Additionally, extrinsic dyes can be covalently attached to proteins.[12] Common extrinsic fluorescent dyes include 8-Anilino-1-naphthalenesulfonate (ANS) and its dimeric analog, 4,4′-bis-1-anilinonaphthalene-8-sulfonate (Bis-ANS) (Figure 6). ANS is barely fluorescent in aqueous environments, but becomes very fluorescent in apolar, organic solvents.[12] ANS interacts favorably with hydrophobic regions of proteins. Such an interaction causes an increase in

fluorescence.[12] Through this hydrophobic binding, ANS is used to monitor folding and unfolding processes of proteins, displaying a substantial increase in fluorescence intensity if an intermediate is present.[12]

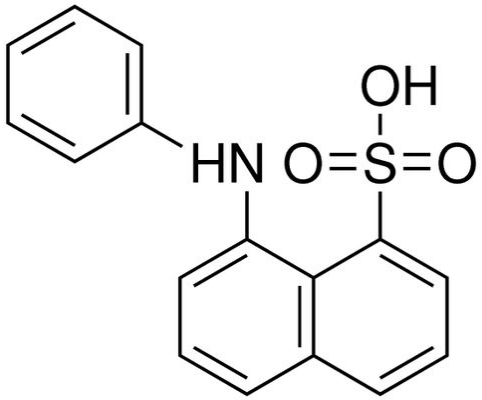

Figure 6. Chemical structure of 8-Anilino-1-naphthalenesulfonate (ANS). ANS is a common extrinsic fluorescent dye that fluoresces when it interacts with hydrophobic regions of proteins. It's dimer, Bis-ANS, acts very similarly, but emits fluorescence at a longer wavelength.

Both ANS and Bis-ANS are sensitive to elements of their environments, including polarity, viscosity, and temperature.[12] Bis-ANS exhibits fluorescent properties similar to those of ANS, but the fluorescence emission of Bis-ANS is at a longer wavelength.[12] For ANS, the primary interaction found between itself and a protein is ion pairing between its negatively charged sulfonate group and positively charged amino acids of the protein (Figure 6).[12] For Bis-ANS, the primary interaction with protein is observed to be hydrophobic.[12] Exposure of hydrophobic surfaces of a protein is marked by an increase in fluorescence intensity due to increased ANS-protein interactions.[12] The interaction of Bis-ANS with solvent-exposed hydrophobic

surfaces on partially unfolded proteins can even help suppress aggregation by sequestering hydrophobic residues and preventing unfavorable interactions between the protein and its hydrophilic environment.[12]

Nuclear Magnetic Resonance

Nuclear magnetic resonance (NMR) spectroscopy is a method used for determining the structure of a protein at the atomic level.[13] While this technique was previously only accessible for the study of smaller proteins, the field has recently advanced to structural studies of high-molecular-weight proteins.[14] It's now used to gain a more complete understanding of the relationship between the structure, motion, and function of a protein through the study of molecular dynamics as it relates to both kinetics and thermodynamics.[14] In an NMR sample, proteins undergo two types of motion as a result of collisions with other proteins and solvent molecules: a random general movement of the entire protein, called Brownian motion, and internal fluctuations at the level of residues, secondary structural elements or domains of a larger protein.[15] NMR can only be performed on a molecule with atomic nuclei that possess net spins.[15] The most abundant nucleus in a protein is that of the hydrogen atom with a spin of +½.[15] Hydrogen's most abundant isotope is most easily visible, but carbon, nitrogen, and oxygen also have isotopes which are spin active.[15] Three-dimensional NMR has been developed, in which three frequency axes exist, each representing a different atomic isotope, for example, ^{1}H, ^{13}C, and ^{15}N.[15]

NMR experiments are carried out in a static magnetic field, B_0, aligned along the z-axis.[15] Interactions between the spins of the various atomic nuclei will depend on their orientations with respect to B_0.[15] Indirect interactions between the two spins are mediated by the atoms' electrons, especially those they share.[15] The ability of NMR to give atomic-level information about molecules is linked to the chemical shift and appearance of peaks, measured in parts per million (ppm) relative to a standard.[13] Each visible peak on the NMR spectrum represents a single interaction, if not multiple overlapping interactions.[15] If a change in the chemical shifts for two particular compounds is observed, this suggests those two compounds are interacting in solution, which is especially applicable to protein-substrate interactions.[15] Stronger peaks represent interactions over shorter distances, while weaker peaks represent interactions over longer distances.[15] Reference values for alpha helices and beta sheets have been assembled from NMR data for each residue type found in the respective secondary structures.[13]

Scalar coupling (J-coupling) is a through-bond interaction between two nuclei that are up to three bonds apart, causing indirect interactions mentioned above.[13] This coupling effect causes NMR signals to be split into multiple peaks.[15] J-couplings are used for computing protein structures, and provide especially useful information regarding the connectivity of the backbone of a peptide.[15] The goal is to determine the location of each labelled functional group with respect to its neighbors until the structure of the entire molecule has been solved.[15] The line

width of NMR peaks increase with the size and rigidity of the molecules. Small peptides produce smaller, narrower signals than large, complex proteins.[15] The line width of NMR spectra can also provide information on the level of aggregation of a protein, since it indicates size.[15] The complex structure of proteins complicates the solution of this puzzle further, since in a folded protein, two labelled protons can be close in space, but not be neighboring residues in the protein's primary structure.[15] Solving only the structure of the protein's backbone gives the location of secondary structural elements. Side chains are more difficult to assign, but their assignment is necessary to solve a complete protein structure.[13]

Fluorescence Resonance Energy Transfer

Spectroscopic imaging techniques like fluorescence resonance energy transfer (FRET) help to identify protein-protein interactions, as well as the accumulation (including numbers of monomers present), colocalization, and conformation of those proteins.[16,17] FRET is also able to monitor molecular movements like sliding and bending.[17] Fluorescence intensity can be measured by spectroscopy or microscopy to obtain information about the state of the protein of interest, however it requires that the protein be labelled, whether chemically or genetically.[16] Genetic labelling is accomplished using gene-encoded fluorescent protein tags in living cells, which is beneficial because it allows proteins to be studied in their physiological environments.[16] FRET refers to the transfer of energy between two of these fluorophore labels.[16] Energy is transferred from the

excited donor fluorophore to the ground state acceptor fluorophore if the two are within a certain distance and are at a certain orientation that represents the interaction of the labelled proteins or molecules being studied (Figure 7). The distance between the two labels must be less than about 10 nm (in three-dimensional space) for efficient energy transfer, and the fluorophores' dipoles should be oriented favorably toward one another (Figure 7).[17] The efficiency of FRET is determined by the percentage of photons released by donor fluorophores than are successfully absorbed by acceptor fluorophores.[17]

A potential experiment would include a donor fluorophore attached to a known and consistent site on the protein, while the position of the acceptor fluorophore is varied.[17] Researchers should be aware of the chance of bystander FRET occurring in studies. In bystander FRET, a signal arises from fluorophores that are in close proximity as a result of random diffusion, rather than their associated proteins interacting.[17] Because of the distance dependence of this technique, FRET can provide information about the distance between molecules or parts of molecules and their respective orientations.[17] FRET provides useful information about the structure of aggregation-prone proteins, like those responsible for neurodegenerative diseases, even if their structures have not been determined by other methods like NMR. [16]

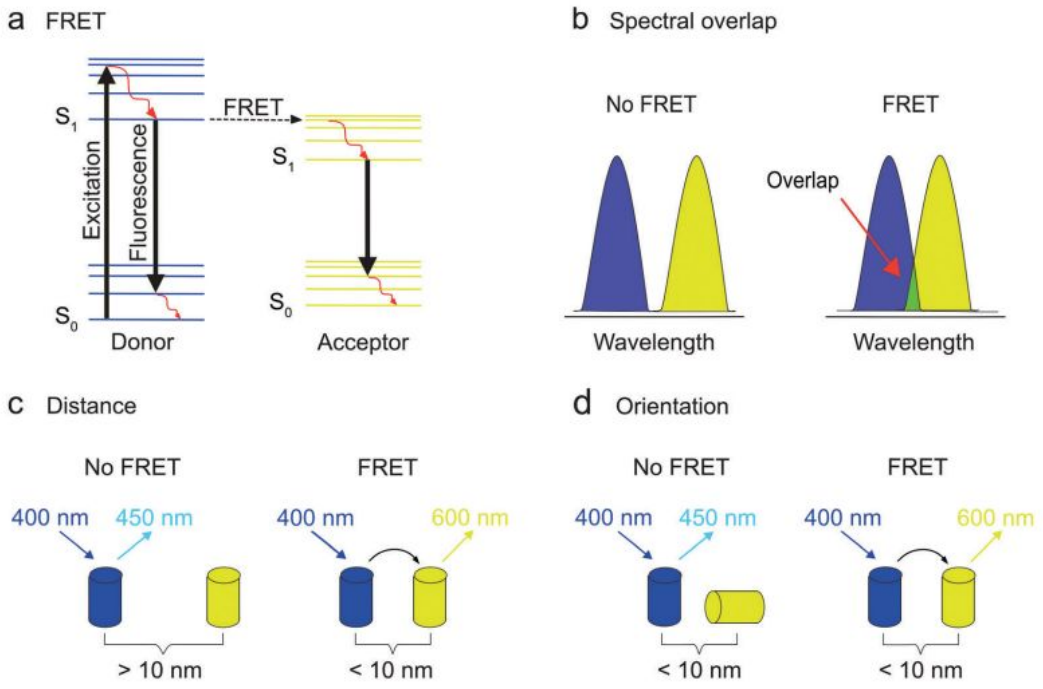

Figure 7. Fluorescence Resonance Energy Transfer detects protein-protein interactions. Fluorescence Resonance Energy Transfer is the transfer of energy between two fluorophore labels attached to proteins. However, the energy transfer and subsequent fluorescence are only successful if the two fluorophores are within a certain distance from one another and are at the proper orientation. This provides information about the structure and function of proteins, both how they fold through self interactions and aggregate through protein-protein interactions. Adapted from Teunissen *et al*., 2018.[17]

Circular Dichroism Spectroscopy

Circular dichroism (CD) spectroscopy is another valuable technique for examining protein structure. CD measures the difference in absorption of clockwise and counter-clockwise circularly polarized light, cumulatively referred to as plane polarized light, after it's passed through the sample of interest.[18] Plane polarized light is split into its two components by being passed through a quartz

crystal modulator with an alternating electric field of 50 kHz.[18] This causes structural changes in the quartz crystal, which in turn creates plane polarized light.[18] CD data is graphed as a function of wavelength to obtain the CD spectrum for a sample.[18] Bands within the spectrum are assigned to distinct structural features, particularly those of secondary structure, within a protein.[18]

In a CD spectrum, peptide bonds absorb light around 240 nm.[18] The amount of regular secondary structures (alpha-helices, beta-sheets, turns) present in a protein appear in the peptide bond region.[18] Aromatic amino acid side chains absorb light between 260 to 320 nm.[18] Each amino acid has its own characteristic absorption profile.[18] Disulfide bonds appear in CD spectra as weak broad bands around 260 nm.[18] A protein's CD spectrum can also provide a fingerprint for its tertiary structure, detect structural changes caused by ligand binding, and measure rates of protein folding.[18] In contrast to NMR, which can give structural information at the atomic level, CD is a low-resolution technique that instead describes overall, primarily secondary, protein structures.[18]

Chromatography

Chromatography is a method often used by biochemists to separate, identify, and purify a specific protein. Depending on the type of chromatography used, proteins can be separated based on properties like size, shape, charge or hydrophobicity.[19] In all forms of chromatography, a mixture containing the protein of interest is applied to a surface and a mobile phase is added.[19] Some components stay longer than others on the stationary phase

based on size or affinity differences, while others enter into the mobile phase and leave the system sooner, leading to the separation of the proteins in the mixture.[19] In stationary phase chromatography, the mobile phase (liquid or gas) flows over the stationary phase.[19]

Column chromatography is the chromatography type most commonly used for separating proteins, particularly to purify them.[19] Samples flow through the column and are collected at the bottom in time- or volume-dependent intervals.[19] Ion exchange chromatography is a subtype of column chromatography based on electrostatic interactions that exist between charged protein groups and a solid matrix.[19] Their opposite charges are used to separate the protein of interest from the mixture. The column-bound protein is then released from the column by changing the pH or ion concentration of the mobile phase.[19] Another subtype of column chromatography is size exclusion chromatography. This method consists of a column packed with dextran-containing material, like gel beads, that can be used to separate macromolecules by size, often to determine a protein's molecular weight.[19] Gel beads contain small pores.[19] Larger molecules that cannot enter the pores of the beads exit the column sooner by passing through the spaces between the beads. Molecules smaller than the beads' pores diffuse through them, entering the beads, leading to a longer retention time on the column.

Affinity chromatography is distinguished by the attachment of a specific ligand to the matrix packing the column. This ligand will bind to the protein of

interest, retaining that protein in the column and allowing all other protein to flow through. Like ion-exchange chromatography, a change in the mobile phase releases the protein of interest from the column.[19] The most recently developed chromatographic category is high-pressure liquid chromatography (HPLC). HPLC passes a mobile phase through a column under 10–400 atmospheres of pressure, and with a flow rate of 0.1–5 cm/sec.[19] High pressure and flow rate increase the separation power of the technique and shorten the separation time.[19]

Isothermal Titration Calorimetry

Isothermal titration calorimetry (ITC) is a biophysical technique, performed in solution and at constant temperature, that measures affinities and enthalpies of specific interactions between proteins, or between a protein and its ligand.[20] It provides information on the purity, solubility, stability, and overall quality of the protein produced by directly determining changes in the enthalpy of reactions.[20] Quantitative information about enthalpy changes can also be used to measure the catalytic activity of proteins acting as enzymes, who do work on their ligands to incur a change. ITC reveals the stoichiometry of a catalytic interaction, as well as the amount of active protein present in the sample.[20] Additionally, ITC can be used to measure the binding constant, K_b, of a protein-ligand binding reaction and can monitor any conformational changes required of both the protein and its ligand in order for their binding to occur.[20] Heat is absorbed or emitted in practically every one of these catalytic interactions, making ITC widely

useful. Understanding the energetics of such interactions are key in formulating a complete understanding of an enzyme's structure-function relationship.[20]

1.3 | Protein Homeostasis

I. Denaturation and Formation of Aggregates

The transformation from a folded protein to a partially unfolded protein can occur in conditions such as lowered pH, increased temperature, or oxidative stress. These conditions indicate cellular stress. Cellular stress is known to cause an increase in the accumulation of protein aggregates.[2] This accumulation, in turn, worsens the state of cellular stress.[2] These environments alter the hydrophobicity and net charge of a protein, resulting in a change in its structure.[2] Beyond environmental conditions, the mutation of a protein can also lead to its aggregation.[21] Once denatured, proteins have an increased chance of forming aggregates through oligomerization of misfolded monomers.[2] For example, alpha-synuclein has been found to undergo increased crosslinking of tyrosine residues under oxidative stress, leading to oligomerization.[2] Oxidative stress has also been shown to increase the phosphorylation of tau proteins, which can facilitate aggregate formation.[2] Similarly, the phosphorylation of amyloid beta at certain residues leads to the formation of oligomers and therefore increased aggregation.[2]

In addition to the conditions mentioned above, the crowded cellular environment itself is a risk for misfolding and aggregation, particularly for

nascent polypeptide chains.[7] The cell has evolved to maintain protein concentrations within the cell that will allow continued solubility of each in physiological conditions.[7] Even with the concentration maintained, a subtle change in a protein's three-dimensional structure can cause it to become unstable and therefore insoluble.[7] Some 15 to 30% of mammalian proteomes (all proteins within the cell) lack ordered structure, either partially or entirely, making them intrinsically disordered proteins (IDPs). IDPs are metastable and therefore even more likely to form the toxic aggregates associated with conformational diseases like Alzheimer's or Parkinson's.[7]

Misfolded proteins typically have hydrophobic residues exposed to solvent. Both folding and aggregation of proteins are driven by hydrophobic forces in an attempt to sequester hydrophobic residues from the aqueous environment of the cytosol.[7] If areas of a protein that are normally separated in the native fold come into contact in order to improve the stability of a misfolded protein, this leads to further misfolding and aggregation, and often a loss of the protein's functionality.[21] Misfolded proteins often form hydrogen bonds with one another to form these stable aggregates.[21] For example, amyloid fibrils are aggregates of amyloid-beta that form hydrogen bonds parallel to the fibrillar axis, with beta-strands lying perpendicular to the axis (Figure 8).[21] Monomers are added to the ends of the amyloid fibril to create an orderly, linear aggregate (Figure 8).[21]

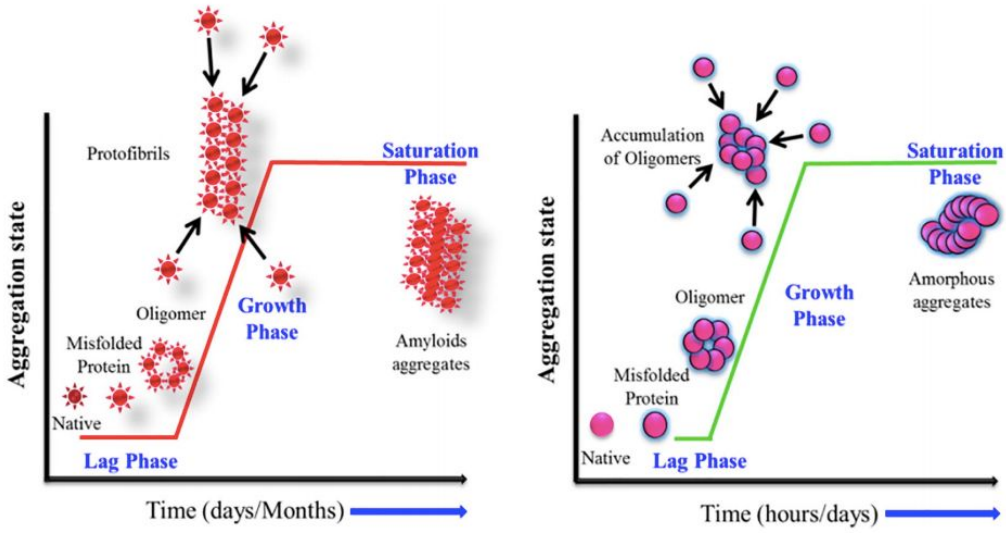

Figure 8. Misfolded proteins bind one another to form stable aggregates. Amyloid fibrils are slow forming. Monomers stack along a singular axis, adding to either end to form the fibrillar aggregate. Amorphous aggregates form more quickly and exhibit less organization. Amorphous aggregates can grow in any direction as monomers are added to a central nucleus. Adapted from Khan, 2018.[21]

In contrast to amyloid fibrils, amorphous aggregates are non-specific and unpredictable in their growth, since monomer units add to an initial nucleus and can form any shape and size as a result (Figure 8).[21] Because there is no limitation to the manner in which the monomers add together, amorphous aggregates usually form faster and grow larger than amyloid fibrils.[21] The formation of an amorphous aggregate takes minutes to hours to form compared to amyloidogenesis (the formation of an amyloid fibril), which can take days to months.[21]

The response of a cell to protein unfolding and damage involves multiple metabolic pathways, called polypeptide quality control pathways, that lead to

either repair or degradation of damaged proteins, and even the sacrifice of the entire cell through programmed cell death.[22] The pathway taken to repair protein damage is now known to depend on the kind of protein denaturation that has occurred.[23] Protein denaturation consists of the rupturing of intramolecular structure-determining bonds within the protein's native fold, resulting in a loss of solubility, subsequent precipitation, and loss of biological function.[23] Although the precipitation of protein is most observable, often to the naked eye, many less observable but still damaging changes can occur to a protein in solution before it loses solubility altogether.[23] The denaturation process can also be described as a protein's transition from its condensed native structure to a more extended or relaxed configuration.[23] A completely denatured protein would simply be a linear polypeptide chain.[23] The more extreme the level of denaturation, the less likely it is to be reversible.[23] Chaperones facilitate the refolding or degradation process of most denatured cellular proteins.

II. Thermally-Induced Aggregation

As mentioned above, there are several environmental stress conditions that can cause protein misfolding and subsequent aggregation. When cells are exposed to elevated temperatures past a certain threshold, cell death begins to occur.[22] Heat stress is known to be significant at 42ºC.[24] Amorphous aggregates in particular are formed at these high temperatures.[21] Proteins in mammalian cells have evolved to be most stable at physiological

temperatures, and the slightest variation in these temperatures can cause cellular proteins to denature and aggregate, leading to loss of protein function and adding to existing cellular stress.[24] Proteins differ in sensitivity to changes in temperature, as well as in the kinetics of aggregation as a response to heat stress.[24] This sensitivity is represented by overall solubility, which reflects the degree to which proteins are affected by heat stress.[24] Heatstress is particularly damaging when a cell is in its growth phase, during which time damage is extended to the cytoskeleton, organelles, and nucleus.[24] It should be noted that small increases in physiological temperature do have certain benefits in specific circumstances, such as in the case of a fever used to regulate the immune system and protect against infection.[24]

III. Chemically-Induced Aggregation

Heat often produces less extreme changes in protein structure than do chemical denaturants such as urea.[23] Both urea and another notable chemical denaturant, guanidine hydrochloride (GdnHCl), disrupt natively folded proteins, distorting the functional conformation and exposing hydrophobic regions to aqueous solvent.[21] In the case of functional oligomers, GdnHCl dissociates them into monomers and dimers, creating nuclei for the formation of toxic aggregates.[25] To be effective, GdnHCl and urea require high concentrations, in the molar range, to destabilize proteins, and these are not cellularly-relevant conditions.[25] Although both display fairly weak interactions with proteins, the driving

force of GdnHCl-induced denaturation is direct electrostatic interaction, while that for urea is hydrogen bonding between urea and the protein's amide backbone.[25] Additionally, through its interactions with hydrophobic side chains, urea stabilizes misfolded proteins, preventing hydrophobic collapse back into native-like structure.[25] GdnHClis also capable of weakening the hydrophobic effect.[25] GdnHCl ions havebeen shown to line up flat along a hydrophobic surface, forming a coating layer, and increasing the stability of exposed hydrophobic residues by reducing their contact with aqueous solvent.[25] Chemical denaturation can also be accomplished through liberation of the sulfhydryl groups of cysteine residues that often participate in disulfide bridges in native protein folds.[23] This liberation leads to dissociation of protein subunits previously held together by these bridges.[23] Dithiothreitol (DTT) is a chemical denaturant that is only effective if a protein has disulfide bonds, since it targets these specifically, reduces the sulfhydryl groups, and causes partial denaturation of the protein.[26] The degree to which a protein is denatured is highly dependent on the identity of the denaturing agent.[23] Chemical denaturation is an effective *in vitro* method for creating changes in protein structure and function.

IV. Methods for Monitoring Protein Aggregation

Absorbance

Tryptophan and tyrosine residues play an important role in the ultraviolet (UV) absorption of proteins.[27] These residues, along with phenylalanine, display aromaticity (closed cyclic delocalized electron systems) that allows electromagnetic radiation to

promote them to an excited state.[28] The range of wavelengths in which this can occur is called the Ultraviolet/Visible (UV/Vis) spectrum.[28] Since these aromatic hydrophobic residues are localized in the interior of a protein's native fold, the detection of them through UV/Vis absorbance can be used to monitor levels of protein unfolding and aggregation.[28] Changes in absorbance intensity or the wavelength of maximum absorbance signal changes in protein structure, which can be monitored as a function of temperature change or addition of denaturing agent. Results can be connected to the increased exposure of hydrophobic residues and therefore to increased denaturation.[28] Interestingly, lysine has been found to display a UV absorption at 270 nm at high concentrations in aqueous solution at neutral pH.[27] This is thought to be the result of interactions between lysine side chains among aggregates.[27] Another application of the UV/Vis absorbance of proteins is measuring opalescence to analyze stability and aggregation.[28] Opalescence is the hazey character of a solution caused by the wavelength-dependent scattering of particles smaller than the wavelength used.[28] This can be measured according to the intensity of the scattered light at a specific angle to the light path.[28]

Thioflavin T

Thioflavin T (ThT) has become the most commonly used dye to detect amyloid aggregation since its first use in 1959.[21,29,30] When bound to amyloid fibrils, it undergoes a significant increase in fluorescence emission at 480 nm after

being excited at 450 nm.[29] A ThT molecule consists of one benzothiazole and one benzaminic ring connected by, and freely rotating around, a shared C-C bond (Figure 9).[29] Unbound ThT in solution has excitation and emission wavelengths of

Figure 9. Chemical structure of amyloid fibril detector Thioflavin T. Thioflavin T (ThT) is a dye used to detect the presence of amyloid beta aggregation. When bound to these aggregates, ThT undergoes fluorescence emission at 480 nm. The ThT molecule consists of a benzothiazole ring (left) and benzaminic ring (right) connected by a freely rotating carbon-carbon bond. Fluorescence occurs when the rotation of the rings is constricted. Adapted from Peccati *et al*., 2017.[30]

385 nm and 445 nm, respectively.[30] It's believed that during a dye binding assay, the increase in fluorescence upon binding is the result of inhibition of free rotation of the rings.[29] It's possible that the intensity of the fluorescent signal is reflective of amyloid fibrils' ability to prevent free rotation of the rings in the ThT molecule.[29] In the ground state, the angle between the two rings in ThT is approximately 40º.[30] When the molecule absorbs electromagnetic radiation and rises to its excited state, the angle between the two rings expands to 90º.[30] When ThT is bound to amyloid fibrils, it's unable to transition to the 90º position and actually becomes planar, so fluorescence emission is observed.[30] The binding of ThT to amyloid fibrils is primarily driven by π-π stacking, and these interactions

are sufficient to constrain the dye molecule.[30] ThT binds to the shallow grooves of amyloid fibrils which are rich in nonpolar residues, supporting the formation of π-π stacking interactions.[30] Although ThT binds nonpolar residues, it displays little specificity for particular amino acids.[30]

Dynamic Light Scattering

Dynamic light scattering (DLS) is another method that can be used to monitor formation and growth of protein aggregates, especially in the case of amyloid fibrils. DLS provides information about the translational, rotational, and internal motions of particles in solution depending on their size and shape.[31] DLS also produces information about the hydrodynamic radius (R_h) of these moving particles.[31] It can detect proteins from 1 nm to 10 μm in diameter, and can provide information about the relative distribution of differently sized particles in solution.[32] A beam of light is shone at a sample of macromolecules. When this light hits the macromolecules in solution, it is scattered; the DLS instrument then measures the directions and angles of the scattering.[31,33] Protein aggregates cause light scattering with an intensity dependent on the molar mass of the aggregate.[33] DLS can distinguish differences in the sizes of these aggregates, and can also use light scattering results to draw information about the rate of diffusion of the macromolecules in solution.[32,33] The intensity of the scattered light depends on the ratio between the particle size and wavelength. The shorter the wavelength of scattered light, the smaller the particles in solution.[32]

Smaller particles also have a greater speed of diffusion in solution, and that speed can be measured based on intensity fluctuations of light scattering caused by those particles.[32]

1.4 | Key Components of Proteostasis

I. The Proteostasis Network

The conversion of genetic code held by mRNA into a functional protein is fundamental to the life of all cells. One mistake in the translation of a protein can disrupt the cell's proteostasis (homeostasis of proteins). An imbalance in proteostasis is involved in the cause of many different diseases, whether that imbalance be the overproduction of a native cellular protein or the toxic accumulation and aggregation of a misfolded protein.[7,34] Proteostasis, when functioning properly, maintains the appropriate levels of protein synthesis, folding, and degradation.[34-36] The proteostasis network (PN) is made up of approximately 1400 components in mammalian cells that work together to maintain the cell's proteostasis.[7] This includes chaperones, modification enzymes, and targeting factors that bind ribosomes and regulate protein folding.[34] The presence of these molecules is not the same in all cells and tissue types, but is tailored to the specific needs of a particular cell.[36]

Proteostasis begins at the ribosome where protein synthesis can be controlled through modulation of the kinetics of translation (Figure 10, 11).[34]

While it is important to maintain a proper balance of all stages of translation, control of elongation, and therefore protein folding, is most important.[34] As mentioned above, protein folding occurs much more quickly than elongation of a nascent polypeptide chain. To avoid misfolding and allow for controlled co-translational folding, the rate of elongation differs along the length of the mRNA transcript (Figure 11).[34] There is evidence that the slowing of translation allows the exit channel of the ribosome to constrain the emerging polypeptide, ensuring it begins along the most efficient folding pathway (Figure 10).[34] The exit channel of the ribosome's large subunit can hold 30 to 40 amino acids of the nascent polypeptide chain. [34] The ribosome then recruits proteostasis machinery to assist with further protein folding if necessary.[34] This recruitment is accompanied by further slowing of the elongation process.[34]

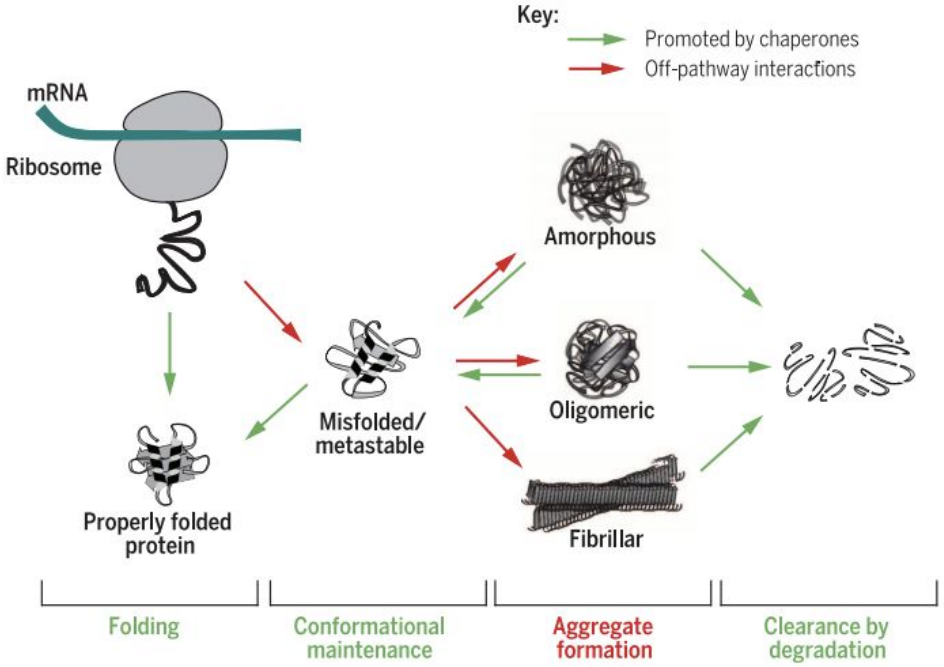

Figure 10. Proteostasis and nascent polypeptides. The proteostasis network begins monitoring protein folding before the polypeptide chain has even been released from the ribosome, since the polypeptide is at risk for misfolding as soon as it emerges from the exit channel of the ribosome. Proteostasis machinery guides the polypeptide along the pathway to its properly folded structure, discouraging it from acquiring misfolded states. Misfolded proteins are at risk for forming several types of aggregates, and this often leads to the protein's degradation. Adapted from Balchin *et al*., 2016.[7]

The speed of translation is also dependent on the availability of necessary tRNAs.[34] tRNA production is therefore another balance of supply-and-demand the proteostasis network needs to monitor. The pool of available tRNAs is dynamic, changing with the needs of the cell.[34] Slowing of the elongation process will decrease protein production, while fast translation increases protein production at the expense of increased risk for errors, misfolding, and aggregation of the nascent polypeptides (Figure 11).[34] Changes in cellular conditions can alter these

balanced translation kinetics.[34] The proteostasis network is also responsible for ribosome recycling and breakdown of unneeded mRNA transcripts.[34] Cellular proteins can be degraded in one of two ways: either by the ubiquitin proteasome system (UPS) or by autophagy, which are both composed of molecules considered part of the cell's PN.[1,36] Most short-lived proteins are degraded by UPS, while proteins with longer lifespans are degraded by autophagy in the lysosome.[1]

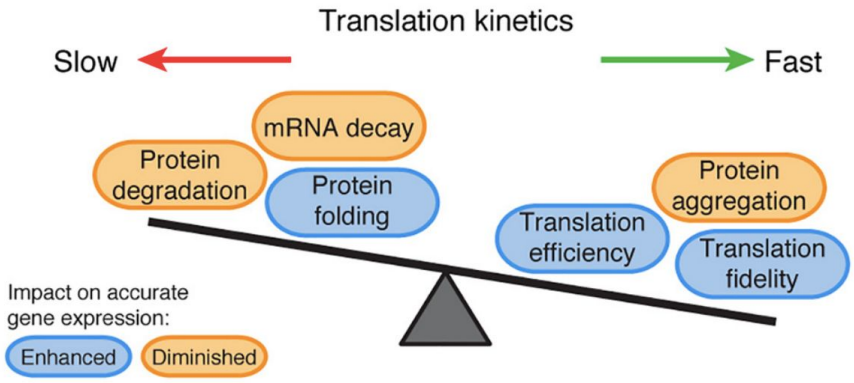

Figure 11. Balance of protein production and degradation is maintained by translation kinetics. The speed of translation can be modulated based on cellular needs. Slowing translation favors correct protein folding, allowing small sections of nascent polypeptide to stabilize as they emerge from the exit channel of the ribosome. This lowers the level of protein degradation occurring, since there are fewer misfolded proteins being produced. Fast translation speeds produce many copies of protein that may be needed for cellular functions, but compromise quality, risking errors and misfolding. Adapted from Stein and Frydman, 2019.[34]

II. Chaperones in Proteostasis

Chaperones are a main component of the cell's PN and its maintenance of cellular and organismal function.[7] Chaperones interact with cofactors and with translation machinery to coordinate the PN.[7] Chaperones facilitate protein folding, conformational repair, and protein degradation through either UPS or autophagy.[7]

When a protein is terminally misfolded or has formed aggregates that are beyond rescue, a molecular chaperone mediates protein degradation .[7] When assisting in protein folding, chaperones stabilize and assist another protein in reaching its functional conformation.[7] Although there is evidence of smaller proteins (< 100 amino acids) refolding on their own when returned from denaturing to favorable conditions, folding and refolding are both less efficient for larger proteins.[7] During protein folding, chaperones work to prevent incorrect intramolecular interactions, which, if stable, are often irreversible.[7] Sometimes a chaperone begins acting on a nascent polypeptide chain before it has fully emerged from the ribosome.[7] Approximately 30% of proteins in the eukaryotic proteome are still unable to fold with the help of ribosome-associated chaperones, and are next passed on to a family of proteins called Heat Shock Proteins (Hsps), where the canonical human chaperone is Hsp70.[7] Hsp70 serves as a hub to receive and relay misfolded substrate proteins to downstream, more specialized chaperones.[7] The Hsp organizing protein (Hop) transfers the substrate from Hsp70 to the next Hsp, a member of the Hsp90 family.[7] If chaperones cannot refold individual proteins, those proteins are ubiquitinated and directed by co-chaperone complexes to the proteasome for degradation.[36,37] When interacting with large protein aggregates, chaperones will release single misfolded proteins from the aggregates if possible.[36] These single proteins are then sent to the proteasome for degradation.

The composition of PN machinery in the cell is dynamic, with adjusting levels of chaperones, co-chaperones, and degradation machinery cell-wide or compartment-specific to meet specific cellular needs.[36] The heat shock response (HSR) is regulated by heat-shock transcription factors (HSFs), altering levels of PN components both in the cytosol and nucleus.[36] When heat shock occurs it causes increased levels of misfolded proteins. Heat shock transcription factor 1 (HSF1) is then activated in the cytosol and rapidly translocated to the nucleus where it binds DNA to turn on expression of chaperone-encoding genes.[36] Once cellular stress from heat shock is relieved, HSF1 is repressed through binding by abundant molecular chaperones.[36] Molecular chaperones in all families are potential targets in treatments for neurodegenerative disorders, since their failure to function allows misfolding and aggregation of proteins.[35] One suggested strategy to increase chaperone activity in cells affected by neurodegenerative diseases has been to artificially activate the heat shock response.[35]

III. The Hsp Families and the Role of ATP

Hsp70 and Hsp90 are highly abundant, making up 1 to 2% of all protein in some cell types, even under non-stress conditions.[36,37] Co-chaperones, such as Hop, which forms a bridge between the two chaperones as mentioned above, can interact with both Hsp70 and Hsp90 to carry out ubiquitination of their bound substrates, marking them for degradation.[36] Hsp90 is able to associate with over 20 different co-chaperones. If interacting with more than one

of these co-chaperones at a time, their combinations can determine Hsp90's function.[36] Recruited by the ribosome-associated complex (RAC), Hsp70 interacts with its substrates early on in the protein folding process, but is also a major component of protein refolding after heat-related cellular stress.[35,37] Sometimes several rounds of binding and release are required by Hsp70 for its substrate to reach its native structure.[36] If Hsp70 fails to correct the fold of its substrate, the substrate is passed on to a protein in the chaperonin (Hsp60) family.[35] Chaperonins are cylindrical enzymes that capture and fold single-chain polypeptides, sequestering them into an environment favorable for folding. In contrast to Hsp70, Hsp90 acts on its substrates later in the folding process.[35,38]

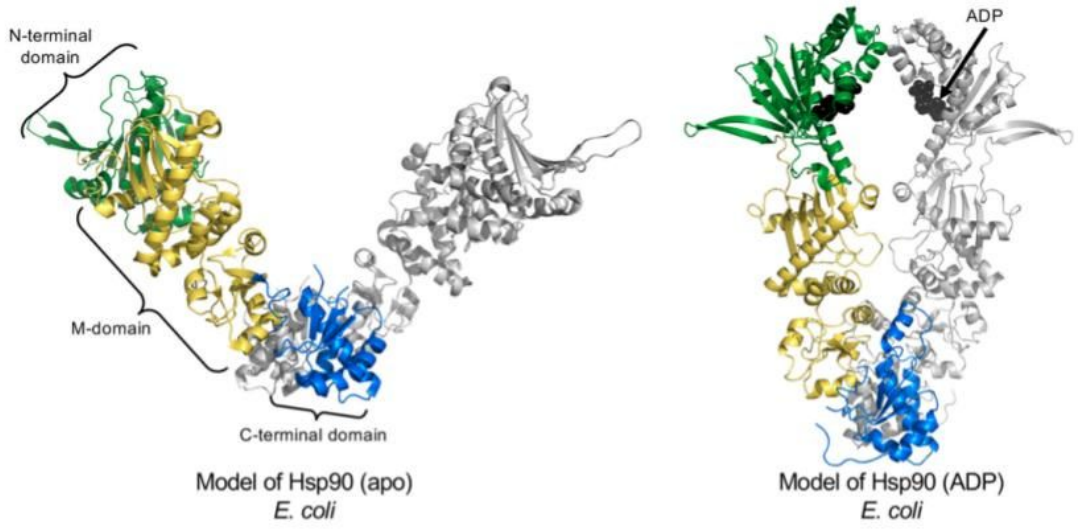

Figure 12. Structure of Hsp90 in two ATP-dependent conformations. The chaperone protein Hsp90 recognizes exposed hydrophobic residues on misfolded substrate proteins. After binding its substrate, Hsp90 either perform "holdase" or "foldase" activity. With no ATP bound, Hsp90 is in the open conformation (left). Upon binding ATP, Hsp90 adopts the closed conformation (right). Hydrolysis and release of ATP causes Hsp90 to return to the open conformation. Adapted from Genest *et al*., 2019.[39]

Hsp70 and Hsp90 are ATP-dependent chaperones.[37] The binding site of Hsp70 is hydrophobic and recognizes hydrophobic stretches on its substrates of up to five residues.[37] Typically, these hydrophobic residues would be sequestered in the core of the substrate protein, unavailable for chaperone recognition. Hsp90 exists in the cytosol as a homodimer with multiple substrate binding sites that undergo large conformational changes.[39] Upon binding ATP, Hsp90 adopts a closed conformation.[39] After ATP is hydrolyzed and ADP is released, Hsp90 shifts back to its open conformation.[39] Often more than one cycle of

ATP/substrate binding and release is needed to return a substrate to its native fold.[7] In addition to its "foldase" ATP-dependent activity, Hsp90 also exhibits "holdase" ATP-independent activity where it binds a substrate to prevent its aggregation, but does not correct its fold.[39] After acting as a "holdase" under stress conditions, Hsp90 will release its substrate, at which time the substrate will often return to its native fold since conditions have returned to normal.[39] Hsp70 exhibits similar structural changes to Hsp90, where large conformational changes occur during an ATP cycle. Hydrolysis of ATP increases Hsp70's affinity for its substrate.[37,39] Hsp70's conformational changes are regulated by interactions with ATP/ADP, co-chaperones, and its substrate.[39]

ATP-independent chaperones, like small heat shock proteins (sHsps), do not actively refold their substrates, but display "holdase" ability, which is characterized by recognizing and binding to misfolded proteins to prevent their aggregation.[38] sHsps are involved in proteostasis by facilitating the refolding of substrates by larger Hsps.[36] Evidence suggests Hsp70 displaces and releases bound sHsps from the surface of the substrate.[40] sHsps carry out this facilitation by forming large, homooligomers that sequester misfolded substrates and prevent them from forming aggregates.[36] Although the full extent of sHsp substrates are unknown, it is known that sHsps act broadly, binding to a wide variety of proteins numbering in the hundreds.[36,40] Their role in the greater PN is also not fully understood, nor is their role in the degeneration of the PN that leads to the

development of conformational diseases.[38] Studies suggest both over and under expression of sHsps can lead to these diseases.[40]

1.5 | Small Heat Shock Proteins

I. Human sHsps: Structure

There are 10 human sHsps, labelled HspB1 through HspB10, all of which reside in the cytosol of cells.[38] All 10 share a general structure consisting of a highly conserved central alpha-crystallin domain (ACD) of approximately 80 amino acids, flanked by less conserved N- and C-terminal regions, denoted NTR and CTR, respectively, that vary in length.[38] A sHsp monomer has a relatively low molecular weight, ranging from 15 to 40 kDa.[38] The ACD's fold is compact, consisting of a beta-sandwich and two antiparallel beta-sheets.[40] The flexible CTR is made up of no more than 20 amino acids, most of which are polar in character and exposed to the solvent.[40] The NTR is highly variable in both sequence and length, but evidence suggests it plays a significant role in both oligomer formation and substrate interactions.[40] In support of the NTR's role in oligomerization, the ACD alone has been found to be unable to successfully oligomerize. Not only is the NTR confirmed to have involvement in substrate binding and oligomerization, but the CTR has been found to be a common linker between two sHsp monomers within an oligomer.[40] The fact that the NTR is often unable to be solved in sHsp crystal structures confirms the NTR's high level of flexibility.[40] In contrast to the CTR, the NTR has many

hydrophobic amino acids, particularly phenylalanines and tryptophans.[40] It's still unknown exactly what portion of the sHsp interacts with and binds a substrate.[40] Since the sHsp-substrate interaction depends on the charge and polarity of the substrate, it is suggested that this interaction can occur on multiple sites within the sHsp.[40]

HspB1 (Hsp27) is arguably the most widely expressed human sHsp, and was one of the first human sHsps to be purified and characterized.[41] When mutated, the disrupted activity of HspB1 has a significant role in the development of conformational diseases.[41] It has three phosphorylation sites at Ser-15, Ser-78, and Ser-82, which are all within its NTR (Figure 13).[40] Its phosphorylation leads to the breakdown of larger oligomers into tetramers, which further dissociate into dimers.[40] It's the addition of negative charges when phosphorylation occurs that disrupt the monomer-monomer interfaces, leading to dissociation.[40] Phosphorylation regulates the presence of oligomers of various sizes in the cell, giving the PN the ability to respond to different cellular environments and events of stress.[41] Evidence suggests oligomers with specific levels of phosphorylation are able to interact with different substrate proteins.[41]

Figure 13. Primary structure of HspB1. HspB1 is a human small heat shock (sHsp) protein found in almost all cells in the body. HspB1 exhibits the general sHsp structure consisting of a conserved central alpha-crystallin domain and variable N- and C-terminal regions. The N-terminal region contains three phosphorylation sites at Ser-15, Ser-78 (not shown), and Ser-82. Phosphorylation of these sites has been shown to lead to dissociation of large oligomers of the sHsp. Adapted from Zhu and Reiser, 2018.[42]

HspB4, also known as alpha-Crystallin A (CryAA), is present in the eye lens along with HspB5 (alpha-crystallin B), and the two form heterooligomers.[40] Together they are believed to maintain the transparency of the eye lens by preventing the aggregation of proteins that leads to cataracts.[40] The cytoplasmic HspB4/HspB5 oligomer exhibits chaperone activity under cellular stress, binding to proteins to stabilize them and prevent their denaturation.[42] The HspB4/HspB5 complex is also known to interact with and stabilize elements of the cytoskeleton, prevent the generation of reactive oxygen species (ROS), as well as translocate to the nucleus to regulate gene expression.[42] Both HspB1 and the HspB4/HspB5 complex have been shown to interact directly with, and inhibit, cellular components involved in apoptosis.[42] HspB4 has two phosphorylation sites: Ser-122 and Ser-148 (Figure 14).[42]

Figure 14. Primary structure of HspB4. HspB4 (also known as alpha-crystallin A) is a human small heat shock protein (sHsp) found in the eye lens. It has been found to exhibit the general sHsp structure consisting of a conserved alpha-crystallin domain and variable N- and C-terminal regions and to form hetero-oligomers with HspB5 (alpha-crystallin B). HspB4 has two phosphorylation sites: one at Ser-122 and one at Ser-148. The first is located in its alpha-crystallin domain and the second in its C-terminal region. Adapted from Zhu and Reiser, 2018.[42]

II. Human sHsps: Function

The capture of unfolded proteins by sHsps is the cell's first line of defense in preventing aggregation under stress (Figure 15).[40] Studies have shown that sHsp-substrate complexes are formed when sHsps are in excess. If the substrate is in excess, sHsps become incorporated into the large aggregates of substrates and are not thought to be functional.[40] Many sHsps form oligomers in solution. For example, HspB5 can form oligomers made up of 24 to 33 monomers.[38] Mammalian sHsp oligomers are known to be dynamic, rapidly changing in size, exchanging monomers of both the same and different sHsps to form both homo- and heterooligomers.[38] These large oligomers act as reservoirs of sHsps (Figure 15).[38] Dimers that have dissociated from larger oligomers display "holdase" chaperone activity, binding to aggregation-prone proteins.[38] It is thought that these smaller forms gain chaperone activity when dissociated due to an increase in exposed hydrophobic regions, which increase their affinity for misfolded

substrates.[38] After complexing with sHsps, substrate proteins can either be transported for degradation or held in a stabilized form until refolded by an ATP-dependent chaperone (Figure 15).[38] The details of how sHsps pass their substrates on to these larger Hsps remains unknown.[38]

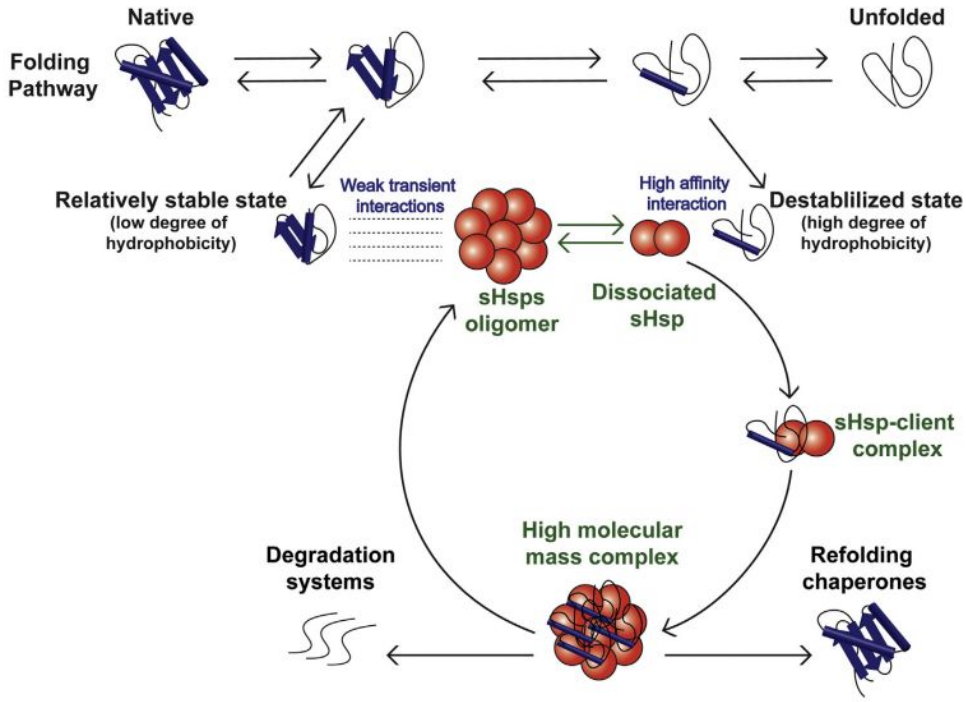

Figure 15. Chaperone-like activity of sHsps. When misfolded proteins are detected in the cell, sHsps complex with them to prevent further misfolding and aggregation from occurring. sHsps are present in the cell in oligomers that are thought to act as reservoirs of sHsp monomers and have no chaperone activity. Dimers dissociate from large oligomers to carry out their "holdase" function on misfolded substrates. sHsps then pass on their substrates to ATP-dependent chaperones that can refold the substrate or mark it for degradation. Adapted from Johnston *et al*., 2018.[38]

1.6 | Model Substrates

I. Insulin

The insulin protein was first isolated in 1921, which led to a subsequent life-saving treatment for people with diabetes. We now refer to these people as insulin-dependent diabetics because they must administer insulin several times a day, but before the insulin protein was able to be mass produced and sold, these people had no effective treatment for their condition.[43] In 1955, insulin was the first protein to have its primary structure sequenced.[43] Insulin was used as a model protein in many of the original findings about protein properties and structure.[43] Insulin circulates through the bloodstream as a monomer, which is its biologically active form.[43] It modulates blood glucose levels by stimulating the uptake of glucose by cells to be broken down for energy. In addition to its central role in metabolism, insulin has since been found to be involved in growth, homeostasis, and reproductive function and longevity.[43] The structure of insulin consists of two polypeptide chains: chain A is 21 amino acids long and chain B is 30 amino acids long.[43] These chains make up three alpha-helices and are connected by two disulfide bridges (Figure 16).[43] Insulin forms dimers, and in the presence of zinc ions, can further oligomerize into hexamers.[43] Insulin hexamers exhibit negative cooperativity where insulin dissociates from cell receptors at an increased rate as the concentration of insulin increases.[43] Under cellular stress conditions like heat,

low pH, or presence of chemical denaturants, insulin is known to form amyloid-like aggregates consisting of beta-sheets.[45]

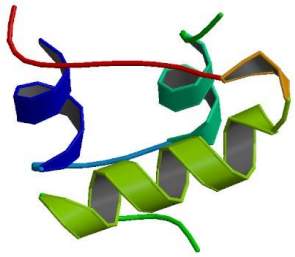

Figure 16. Structure of the model substrate protein insulin. Since its early discovery, insulin as been used as a model for many developments of scientific knowledge. In the body, insulin functions to modulate blood glucose levels. Errors with insulin production or cellular reception of the protein lead to diabetes. The structure of insulin consists of two polypeptide chains that form three alpha-helices. Adapted from Timofeev *et al*., 2010.[44]

II. Lysozyme

Lysozyme is a globular protein with the ability to lyse bacteria.[46] As a bacteriolytic enzyme, lysozyme cleaves beta-1,4-glycosidic linkages in the peptidoglycan cell wall of bacterial cells.[46] In humans, lysozyme is present in high concentrations in the liver, saliva, and tears, as well as in several types of immune cells, helping us to fight off infections.[46] Human lysozyme consists of 130 amino acids folded into two domains: an alpha domain made up of four alpha-helices and a beta domain made up of an antiparallel beta-sheet and a long loop (Figure 17).[46] The active site in lysozyme is located in the cleft between the two domains.[46] Mutations in lysozyme can lead to the loss of most alpha-helical

structure, increased presence of beta-sheets, and the formation of amyloid-like aggregates, as can conditions of high heat.[46]

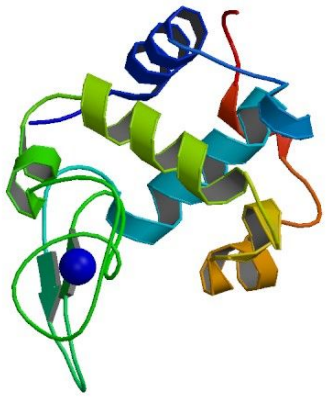

Figure 17. Structure of the bacteriolytic enzyme lysozyme. Lysozyme cleaves beta-1,4-glycosidic linkages in the peptidoglycan cell wall of bacteria, contributing to the body's immune response. Lysozyme consists of two domains: one made up of four alpha-helices and one of an antiparallel beta sheet and a long loop. The active site is located between these two domains. Adapted from Shoyama *et al* ., 2009.[47]

III. Malate Dehydrogenase

Malate dehydrogenase (MDH) plays a key role in the malate-aspartate shuttle across the mitochondrial membrane in the citric acid cycle, part of the metabolic pathway for aerobic organisms.[48] The shuttle transports reducing equivalents into the mitochondria in the form of malate, since NADH can't cross alone.[48] MDH specifically catalyzes the NAD^+-dependent conversion between malate and oxaloacetate inside the mitochondria, producing oxaloacetate and reduced NADH.[48] High concentrations of malate stimulate the production of oxaloacetate, while high concentrations

of oxaloacetate inhibit MDH through allosteric binding.[48] The structure of MDH is highly conserved across eukaryotes and most bacterial species.[48] It has a length of about 350 amino acids, varying only slightly between species, and exists in solution as a dimer (Figure 18).[48] Each monomer has two domains: an

Figure 18. Structure of human malate dehydrogenase type 2. Malate dehydrogenase (MDH) type 2 is localized in the mitochondria. It converts malate to oxaloacetate after malate has been shuttled into the mitochondria and has reduced NADH. MDH exists in solution as a dimer. Each monomer has two domains, one for binding NAD^+ and one for binding malate. The NAD-binding domain has a Rossmann fold motif, while the malate-binding domain has four beta-sheets and one alpha-helix. Adapted from Ugochukwu *et al* ., 2006.[49]

NAD^+-binding domain near the protein's NTR and a substrate-binding domain with catalytically active amino acids near the CTR.[48] The NAD^+-binding domain is made up of a specific parallel beta-sheet structure called a Rossmann fold motif and the substrate-binding domain is made up of four beta-sheets and one alpha-helix (Figure 18).[48] The dimer interface, where the two monomers meet, consists mainly of alpha-helices packed tightly together.[48] This interface is stabilized by hydrogen bonds and hydrophobic interactions.[48]

IV. Citrate Synthase

Like MDH, citrate synthase (CS) also plays a key role in the citric acid cycle, as the only enzyme in the cycle that catalyzes the formation of a carbon-carbon bond.[50] CS produces two reducing equivalents to be transported to the electron transport chain or to be used in the synthesis of amino acids.[50] To do so, it also converts acetyl-Coenzyme A (acetyl-CoA) to citrate, though it must bind oxaloacetate first to increase its binding affinity for acetyl-CoA.[50] The enzyme's turnover number, reflecting its efficiency, is approximately 6000 $mol \cdot sec^{-1}$ per active site.[50] CS also displays high specificity for its substrates.[50] CS isolated from the mitochondria of porcine heart cells is often used

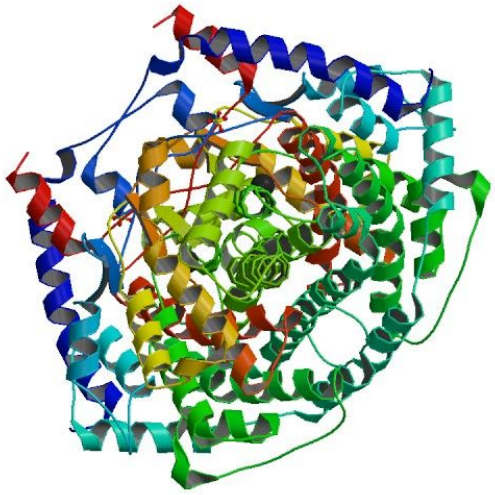

Figure 19. Structure of model substrate citrate synthase from porcine heart. Citrate synthase (CS) plays a key role in the citric acid cycle, where it converts acetyl-CoA to citrate, forming two reducing equivalents. CS consists of two monomers, each with two active sites: one that binds oxaloacetate and one that binds acetyl-CoA. It's structure is made up of 20 alpha-helice, one small beta-sheet, and several disordered regions. Adapted from Larson *et al*., 2009.[51]

as a model substrate for scientific research. The enzyme consists of two monomers totalling 437 amino acids and summing to a total molecular weight of 48,969 Da (Figure 19).[50] Each monomer has an active site that binds one oxaloacetate and one acetyl-CoA, and consists of 20 alpha-helices (Figure 19).[50] The remainder of the protein structure is irregular except for a beta-sheet made up of only 13 amino acids (Figure 19).[50] Studies have suggested that the monomers' active sites function independently of one another and do not bind substrates in a cooperative manner.[50] In the absence of either ligand, CS is in an open conformation, but adopts a closed conformation in the presence of either oxaloacetate or acetyl-CoA through the rotation of its two domains with respect to one another.[50] This shift suggests that acetyl-CoA is unable to bind CS in its alternate conformations, in support of the induced fit model of enzyme catalysis.[50]

1.7 | Approaches in Chemical Biology Using Gold Nanoparticles

Gold nanoparticles (AuNPs) have unique chemical and physical properties that show exciting promise in several fields. Of particular relevance is the development of AuNP uses in the medical field as a drug or bioactive agent delivery system. AuNPs ranging in size from 0.2 to 100 nm have large surface to volume ratios, as well as useful optical, electrical, magnetic, and catalytic abilities.[52,53] These properties are dependent on AuNPs' size and shape, which can be monitored especially easily by observing color differences in solution (Figure 20).[52] Changes in degree of dispersal or aggregation of AuNPs

in solution is also visible through color changes.[52] Size, shape, and particularly diameter have large effects on the stability and function of nanoparticles (NPs) (Figure 20).[53] In addition to three-dimensional NPs, nanomaterials are also being developed in the form of thin, one-dimensional films and two-dimensional nanotubes.[53] Some studies suggest that AuNPs have good biocompatibility due to signs of low toxicity, antibacterial properties, and easy abilities to be imaged *in vivo*.[52] Other studies suggest reasons to be concerned about AuNP-related health risks. It has been shown that exposure to NPs causes toxicity, apoptosis, oxidative stress, and even lung inflammation.[53] Another challenge has arisen during AuNP synthesis in controlling size and maintaining stability.[53]

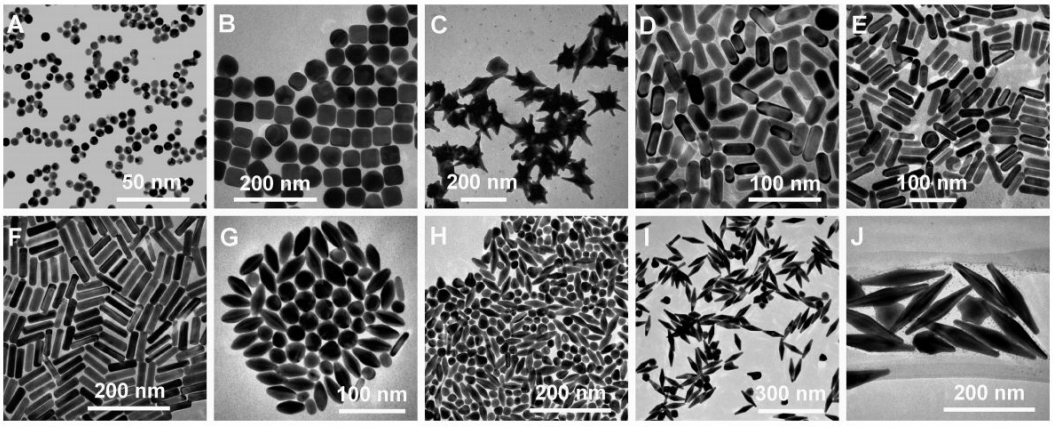

Figure 20. Diversity of gold nanostructures. The properties of gold nanoparticles (AuNPs) depend on their size and shape. Several examples of different nanostructures are shown. **(A)** nanospheres, **(B)** nanocubes, **(C)** nanobranches, **(D-F)** nanorods of various sizes, **(G-J)** nanobipyramids of various sizes. Adapted from Vines *et al*., 2019.[54]

Despite potential risks, research has moved forward in characterizing benefits to be reaped from NPs, gold or otherwise. Their incredibly small size allows them to pass through the blood brain barrier (BBB), which opens up the possibility for their use in the treatment of neurodegenerative diseases, like Alzheimer's.[21] AuNP-mediated assays have been developed that take advantage of their favorable imaging properties to detect the presence of metal ions, nucleic acids, and proteins.[52] Small molecules, such as amino acids and sulfur-containing compounds, are being conjugated to the surface of AuNPs, as are larger macromolecules, though with more risk of steric hindrance and unwanted interactions.[52]

Of special interest in the medical field concerning treatment development is the property displayed by AuNPs called stimuli response release, which can be used to control the release of drugs when they reach certain physical or chemical environments based on temperature, magnetic field, pH, or light.[53] Potential treatments can also take advantage of the antimicrobial properties of AuNPs mentioned above. AuNPs can target microbes by damaging their DNA, inhibiting DNA replication and protein synthesis, and damaging the microbe's cell wall or plasma membrane.[53] AuNPs can be beneficial for the progress of cancer treatments by potentially solving the issue of nonspecific drug distribution through use of controlled drug release targeted only to cancerous cells.[53] Nonspecific drug distribution affects healthy cells as well as cancerous ones, causing the severe side effects associated with today's cancer treatments.[53] Other

drug-associated benefits of AuNPs include enhanced solubility of hydrophobic drugs, prolonged circulation time, and enhanced cellular penetration.[53]

We have studied the structure and function of small heat shock proteins using many of the concepts and tools of protein biochemistry and chemical biology explained above. Our work has been focused on characterizing the interactions between sHsps and their substrates. We have sought answers to questions concerning substrate specificity, probed isolated regions of sHsps thought to be involved in substrate binding, and integrated nanoparticles as peptide scaffolds to evaluate facilitation of sHsp chaperone-like activity. This was all in an attempt to improve understanding of the role sHsps play in the maintenance of proteostasis and to contribute to their potential use as therapeutic agents for conformational diseases.

Chapter 1 References

1. Zerovnik, E. Protein Conformational Pathology in Alzheimer's and Other Neurodegenerative Diseases; New Targets for Therapy. *Current Alzheimer Research* **2009***, 999*, 1-6.
2. Choi, M. L.; Gandhi, S. Crucial role of protein oligomerization in the pathogenesis of Alzheimer's and Parkinson's diseases. *Febs J.* **2018***, 285*, 3631-3644.
3. Braak, H.; Del Tredici, K.; Rüb, U.; De Vos, R. A.; Steur, E. N. J.; Braak, E. Staging of brain pathology related to sporadic Parkinson's disease. *Neurobiol. Aging* **2003***, 24*, 197-211.
4. Ahlschwede, K.; Omtri, R.; Kandimalla, K. Role of Nanotechnology in the Diagnosis and Treatment of Alzheimer's Disease. In 2012; pp 107-124.
5. Longhena, F.; Faustini, G.; Spillantini, M. G.; Bellucci, A. Living in Promiscuity: The Multiple Partners of Alpha-Synuclein at the Synapse in Physiology and Pathology. *International journal of molecular sciences* **2019***, 20*, 141.
6. Sveinbjornsdottir, S. The clinical symptoms of Parkinson's disease. *J. Neurochem.* **2016***, 139*, 318-324.
7. David Balchin; Manajit Hayer-Hartl; F Ulrich Hartl In vivo aspects of protein folding and quality control. *Science (New York, N.Y.)* **2016***, 353*, aac4354.
8. Moldave, K. EUKARYOTIC PROTEIN SYNTHESIS. *Annu. Rev. Biochem.* **1985***, 54*, 1109-1149.
9. Rossmann, M. G.; Argos, P. Protein folding. *Annu. Rev. Biochem.* **1981***, 50*, 497-532.
10. Finkelstein, A. V. 50 years of protein folding. *Biochemistry (Moscow)* **2018***, 83*, S18.
11. Zhou, H.; Pang, X. Electrostatic interactions in protein structure, folding, binding, and condensation. *Chem. Rev.* **2018***, 118*, 1691-1741.
12. Hawe, A.; Sutter, M.; Jiskoot, W. Extrinsic fluorescent dyes as tools for protein characterization. *Pharm. Res.* **2008***, 25*, 1487-1499.
13. Wüthrich, K. Protein structure determination in solution by NMR spectroscopy. *J. Biol. Chem.* **1990***, 265*, 22059-22062.
14. Kay, L. E. NMR studies of protein structure and dynamics. *Journal of Magnetic Resonance* **2011***, 213*, 477-491.
15. Marion, D. An introduction to biological NMR spectroscopy. *Molecular & Cellular Proteomics* **2013***, 12*, 3006-3025.
16. Kitamura, A.; Nagata, K.; Kinjo, M. Conformational analysis of misfolded protein aggregation by FRET and live-cell imaging techniques. *International journal of molecular sciences* **2015***, 16*, 6076-6092.
17. Teunissen, A. J.; Pérez-Medina, C.; Meijerink, A.; Mulder, W. J. Investigating supramolecular systems using Förster resonance energy transfer. *Chem. Soc.*

Rev. **2018***, 47*, 7027-7044.
18. Kelly, S. M.; Jess, T. J.; Price, N. C. How to study proteins by circular dichroism. *Biochimica et Biophysica Acta (BBA)-Proteins and Proteomics* **2005***, 1751*, 119-139.
19. Coskun, O. Separation techniques: chromatography. *Northern clinics of Istanbul* **2016***, 3*, 156.
20. Baranauskiene, L.; Kuo, T.; Chen, W.; Matulis, D. Isothermal titration calorimetry for characterization of recombinant proteins. *Curr. Opin. Biotechnol.* **2019***, 55*, 9-15.
21. Khan, M. V.; Zakariya, S. M.; Khan, R. H. Protein folding, misfolding and aggregation: A tale of constructive to destructive assembly. *Int. J. Biol. Macromol.* **2018***, 112*, 217-229.
22. Zhang, Y.; Calderwood, S. K. Autophagy, protein aggregation and hyperthermia: a mini-review. *International Journal of Hyperthermia* **2011***, 27*, 409-414.
23. Neurath, H.; Greenstein, J. P.; Putnam, F. W.; Erickson, J. A. The chemistry of protein denaturation. *Chem. Rev.* **1944***, 34*, 157-265.
24. Wilkening, A.; Rüb, C.; Sylvester, M.; Voos, W. Analysis of heat-induced protein aggregation in human mitochondria. *J. Biol. Chem.* **2018***, 293*, 11537-11552.
25. England, J. L.; Haran, G. Role of solvation effects in protein denaturation: from thermodynamics to single molecules and back. *Annu. Rev. Phys. Chem.* **2011***, 62*, 257-277.
26. Bumagina, Z. M.; Gurvits, B. Y.; Artemova, N. V.; Muranov, K. O.; Yudin, I. K.; Kurganov, B. I. Mechanism of suppression of dithiothreitol-induced aggregation of bovine α-lactalbumin by α-crystallin. *Biophys. Chem.* **2010***, 146*, 108-117.
27. Homchaudhuri, L.; Swaminathan, R. Near ultraviolet absorption arising from lysine residues in close proximity: A probe to monitor protein unfolding and aggregation in lysine-rich proteins. *Bull. Chem. Soc. Jpn.* **2004***, 77*, 765-769.
28. Blaffert, J.; Haeri, H. H.; Blech, M.; Hinderberger, D.; Garidel, P. Spectroscopic methods for assessing the molecular origins of macroscopic solution properties of highly concentrated liquid protein solutions. *Anal. Biochem.* **2018***, 561*, 70-88.
29. Invernizzi, G.; Papaleo, E.; Sabate, R.; Ventura, S. Protein aggregation: Mechanisms and functional consequences. *Int. J. Biochem. Cell Biol.* **2012***, 44*, 1541-1554.
30. Peccati, F.; Pantaleone, S.; Solans-Monfort, X.; Sodupe, M. Fluorescent Markers for Amyloid-beta Detection: Computational Insights. *Isr. J. Chem.* **2017***, 57*, 686-698.
31. Georgalis, Y.; Starikov, E. B.; Hollenbach, B.; Lurz, R.; Scherzinger, E.; Saenger, W.; Lehrach, H.; Wanker, E. E. Huntingtin aggregation monitored by

dynamic light scattering. *Proceedings of the National Academy of Sciences* **1998***, 95*, 6118-6121.
32. Mahler, H.; Friess, W.; Grauschopf, U.; Kiese, S. Protein Aggregation: Pathways, Induction Factors and Analysis. *J. Pharm. Sci.* **2009***, 98*, 2909-2934.
33. Pryor, N. E.; Moss, M. A.; Hestekin, C. N. Unraveling the Early Events of Amyloid-beta Protein (A beta) Aggregation: Techniques for the Determination of A beta Aggregate Size. *Int. J. Mol. Sci.* **2012***, 13*, 3038-3072.
34. Stein, K. C.; Frydman, J. The stop-and-go traffic regulating protein biogenesis: How translation kinetics controls proteostasis. *J. Biol. Chem.* **2019***, 294*, 2076-2084.
35. Soares, T. R.; Reis, S. D.; Pinho, B. R.; Duchen, M. R.; Oliveira, J. M. A. Targeting the proteostasis network in Huntington's disease. *Ageing Res. Rev.* **2019***, 49*, 92-103.
36. Labbadia, J.; Morimoto, R. I. The biology of proteostasis in aging and disease. *Annu. Rev. Biochem.* **2015***, 84*, 435-464.
37. Luengo, T. M.; Mayer, M. P.; Ruediger, S. G. D. The Hsp70-Hsp90 Chaperone Cascade in Protein Folding. *Trends Cell Biol.* **2019***, 29*, 164-177.
38. Johnston, C. L.; Marzano, N. R.; van Oijen, A. M.; Ecroyd, H. Using Single-Molecule Approaches to Understand the Molecular Mechanisms of Heat-Shock Protein Chaperone Function. *J. Mol. Biol.* **2018***, 430*, 4525-4546.
39. Genest, O.; Wickner, S.; Doyle, S. M. Hsp90 and Hsp70 chaperones: Collaborators in protein remodeling. *J. Biol. Chem.* **2019***, 294*, 2109-2120.
40. Haslbeck, M.; Weinkauf, S.; Buchner, J. Small heat shock proteins: Simplicity meets complexity. *J. Biol. Chem.* **2019***, 294*, 2121-2132.
41. Arrigo, A.; Gibert, B. Protein interactomes of three stress inducible small heat shock proteins: HspB1, HspB5 and HspB8. *Int. J. Hyperthermia* **2013***, 29*, 409-422.
42. Zhu, Z.; Reiser, G. The small heat shock proteins, especially HspB4 and HspB5 are promising protectants in neurodegenerative diseases. *Neurochem. Int.* **2018***, 115*, 69-79.
43. De Meyts, P. Insulin and its receptor: structure, function and evolution. *Bioessays* **2004***, 26*, 1351-1362.
44. Timofeev, V. I.; Chuprov-Netochin, R. N.; Samigina, V. R.; Bezuglov, V. V.; Miroshnikov, K. A.; Kuranova, I. P. X-ray investigation of gene-engineered human insulin crystallized from a solution containing polysialic acid. *Acta Crystallogr. Sect. F. Struct. Biol. Cryst. Commun.* **2010***, 66*, 259-263.
45. Grudzielanek, S.; Jansen, R.; Winter, R. Solvational tuning of the unfolding, aggregation and amyloidogenesis of insulin. *J. Mol. Biol.* **2005***, 351*, 879-894.
46. Merlini, G.; Bellotti, V. Lysozyme: A paradigmatic molecule for the investigation of protein structure, function and misfolding. *Clin. Chim. Acta* **2005***, 357*, 168-172.
47. AnonymousPreparation and characterization of methyonyl-lysine attached

human lysozyme expressed in Escherichia coli and its effective conversion to the authentic-like protein. *TO. BE PUBLISHED* .
48. Minarik, P.; Tomaskova, N.; Kollarova, M.; Antalik, M. Malate dehydrogenases-structure and function. *Gen. Physiol. Biophys.* **2002***, 21*, 257-266.
49. AnonymousCrystal Structure of Human Malate Dehydrogenase Type 2. *TO. BE PUBLISHED* .
50. WIEGAND, G.; REMINGTON, S. J. Citrate Synthase - Structure, Control, and Mechanism. *Annu. Rev. Biophys. Biophys. Chem.* **1986***, 15*, 97-117.
51. Larson, S. B.; Day, J. S.; Nguyen, C.; Cudney, R.; McPherson, A. Structure of pig heart citrate synthase at 1.78 A resolution. *Acta Crystallogr. Sect. F. Struct. Biol. Cryst. Commun.* **2009***, 65*, 430-434.
52. Chen, Y.; Xianyu, Y.; Jiang, X. Surface Modification of Gold Nanoparticles with Small Molecules for Biochemical Analysis. *Acc. Chem. Res.* **2017***, 50*, 310-319.
53. Rudramurthy, G. R.; Swamy, M. K. Potential applications of engineered nanoparticles in medicine and biology: an update. *J. Biol. Inorg. Chem.* **2018***, 23*, 1185-1204.
54. Vines, J. B.; Yvon, J.; Ryu, N.; Lim, D.; Park, H. Gold Nanoparticles for Photothermal Cancer Therapy. *Front. Chem.* **2019***, 7*, 167.

CHAPTER 2 | MATERIALS AND METHODS

2.1 | Characterizing the chaperone-like activity of HspB1 and its NTR

Peptides, Proteins and Reagents. Malate dehydrogenase (MDH) was obtained from EMD Millipore. Lysozyme (Lys) and Citrate synthase (CS) were procured from Sigma Aldrich. HALT protease inhibitor cocktail was purchased from Fisher Scientific. Unconjugated citrate-coated gold nanoparticles (AuNPs), PEGylated gold nanoparticles (PEG-NP), and high and low density purified sHsp-conjugated gold nanoparticles (B1NTR-NP) were obtained from Nano Hybrids (Austin, TX). Prior to HspB1NTR conjugation, a PEG linker was attached to the AuNP to increase NP stability. The resulting NPs were stored in 1x PBS with 0.05% Tween and characterized by DLS and TEM (Supplemental Information Table S1, Figure S4).

Protein Expression and Purification. The N-terminal region (NTR) (residues 1-88) of HspB1 with an inserted N-terminal cysteine (B1NTR) was expressed from the pMCSG7 vector (gifted by Dr. Jason Gestwicki, UCSF). after ligation independent cloning HspB1NTR was designed with an N-terminal cysteine residue for use in several downstream applications. The first was to facilitate the coupling of the peptide to the surface of gold nanoparticles using thiol-gold interactions.[1] In future studies, incorporating a label for B1NTR may be necessary, and the presence of a single cysteine would create a site-specific chemical “handle” for

labeling experiments. Furthermore, wild-type HspB1 does contain a single cysteine within the ACD, indicating the presence of a cysteine residue is not out of place in the context of potential HspB1-substrate interactions. All recombinant sHsps were expressed in *E. coli* BL21 (DE3), cultured in LB media containing 100 μg/mL ampicillin or 50 μg/mL kanamycin (wild-type HspB1), as previously described.[2] Protein expression was induced with the addition of isopropyl thio-β-D-thiogalactoside to a final concentration of 0.5 mM at 25°C for 5 hours. Wild-type HspB1 was purified by methods previously described.[3] Recombinant human HspB1 was expressed in *E. coli* BL21 (DE3) cells using plasmids kindly gifted by Dr. Jason Gestwicki (UCSF). Cells were centrifuged at 11,000 RCF at 4°C for 15 minutes, and then resuspended in lysis buffer (20 mM Tris, 100 mM NaCl, 6 M urea, 5 mM β-mercaptoethanol, 15 mM imidazole, pH 8.0) with the addition of a cocktail protease inhibitor. Resuspended cells were sonicated for 6 intervals of 30 seconds with alternating 30 second breaks. The lysed cells were then centrifuged again at 20,000 RCF and 4°C for 45 minutes. All proteins were purified from lysate using Ni^{2+} affinity columns. Resulting proteins were exchanged into 25 mM sodium phosphate and 100 mM sodium chloride buffer (pH 7.4), then underwent further purification by size exclusion chromatography (SEC) in 1x PBS (pH 7.4). Protein concentration was determined using the Thermo Scientific BCA assay kit and NanoDrop One UV/Vis Spectrometer (Thermo Scientific).

CD-Spectroscopy. B1NTR was diluted to 0.24 mg/mL in PBS. CD spectra were recorded in a Jasco J-1500 Spectrometer (Jasco Co., Tokyo, Japan) at 24°C. Far UV CD spectra were recorded using a cuvette with 1 mm path length at 0.5 nm intervals between 190 and 250 nm. The spectra were taken as the average of 15 scans recorded at a speed of 100 nm/min.

Chaperone-like Activity Assay. To determine whether the N-terminal region of HspB1 modulates chaperone function, B1NTR, B1NTR-NPs, and corresponding controls (HspB1, PEG-NPs, citrate-NPs) were independently mixed with two heat-denatured substrate proteins, MDH and CS. CS aggregation assays were performed using 2.5 μM of substrate in 0.1 mL PBS (pH 7.4) at 45°C, in both the absence and presence of B1NTR, B1NTR-NP, wild-type HspB1, or other indicated controls. MDH aggregation assays were performed using 15 μM of substrate in 0.1 mL PBS (pH 7.4) at 45°C, in the absence and presence of B1NTR, B1NTR-NP, wild-type HspB1, or other indicated controls. The DTT-induced aggregation of Lysozyme (Lys) was also observed in 1x PBS (pH 7.4). Lys (35 μM) was denatured in the presence of 20 mM DTT in a clear bottom 96-well plate. Aggregation was monitored at 340 nm in a Molecular Devices M5e multi-mode plate reader under constant temperature (37°C), while shaking for 10 seconds between each read. All assays were normalized based on the maximum absorbance of the averaged substrate (CS, MDH, Lys) curves.

Chaperone and Substrate Solubility Gel. Samples obtained from the chaperone-like activity assay (0.5 mL) were centrifuged at 13,000 RPM for 3 minutes, repeated twice. The soluble and pelleted fractions were collected separately. Following this, 1x non-reducing sample loading buffer was added to each sample. MDH samples and controls were run on 10% mini-PROTEAN TGX precast gels (Bio-Rad). CS samples and controls were run on 8-16% gradient mini-PROTEAN TGX precast gels (Bio-Rad). Lys samples and controls were run on a 10% mini-PROTEAN TGX precast, stain-free gel. All gels were run for 40 minutes at 160 V. The gels were silver stained according to the protocol specified in the Pierce Silver Stain kit (Thermo scientific).

Size Exclusion Chromatography (SEC). Changes in protein complex size arising from the interaction of B1NTR with substrate proteins were analyzed by SEC. Samples were prepared using equimolar ratios of B1NTR and substrate, as indicated. Concentrations varied for each substrate: 5μM CS, 50μM MDH or 75μM Lys. Each was mixed with indicated amounts of B1NTR. Each sample (1 mL) was heated at 45ºC for one hour, then cooled to room temperature. Following this, 200 μL of each sample was loaded on to a Superdex 200 10/300 increase or Superose 6 10/300 increase column, equilibrated with PBS (pH 7.4) and attached to an AKTA Pure 25 (GE Healthcare, Pittsburgh, PA). The column was run at 4°C with a flow rate of 0.3 mL/min. Previously, each column had been calibrated

with the following protein markers: thyroglobulin (669 kDa), γ-globulin (158 kDa), ovalbumin (44 kDa), myoglobin (17 kDa), and vitamin B12 (1.35 kDa), to generate a standard curve (Supplemental Information, Figure S1).

1,8-ANS (ANS) Binding Studies. A stock solution (20 mM) of 1,8-ANS (1-Anilinonaphthalene-8-Sulfonic Acid, Sigma-Aldrich) was dissolved in DMSO and diluted using 1x PBS to a 100 μM final concentration for each assay. The binding assay was performed by combining B1NTR (15 μM final concentration) with ANS for 1 hour at either 25ºC, 45ºC, or 55ºC. Fluorescence was measured in a 96-well, black, flat-bottom, polypropylene plate (Fisherbrand) on a M5e multi-mode plate reader (Molecular Devices). Solutions were excited at 375 nm and emission intensities were measured from 400 to 600 nm. All values were measured in arbitrary units and were normalized to the highest value for ANS binding to B1NTR at 25ºC. Each curve is the average of ≥ 3 independent trials.

2.2 | Characterizing the chaperone-like activity of mini alpha-crystallin A: CryAAID1

Peptides, Proteins and Reagents. Lysozyme (Lys), Insulin (Ins) and Alpha-Lactalbumin (alpha-Lac) were all obtained from Sigma Aldrich. 5 and 10 nm PEGylated gold nanoparticles (PEG-NP) and purified sHsp-conjugated gold nanoparticles (CryAAID1-NP) were obtained from Nano Hybrids (Austin, TX).

The CryAAID1 peptide (mini alpha-crystallin A), residues 70-88 of alpha-crystallin A (HspB4), was synthesized by Genscript. Prior to CryAAID1 conjugation, a PEG linker was attached to the AuNP to increase NP stability. The resulting NPs were stored in 1x PBS with 0.01% Tween-20 and characterized by DLS (Supplemental Information, Table S1).

Chaperone-like Activity Assay. To determine whether the CryAAID1 peptide of alpha-crystallin A modulates chaperone function, CryAAID1-NPs, with corresponding PEG-NPs as a control, were independently mixed with three DTT-denatured substrate proteins, Lys, Ins, and alpha-Lac. Lys aggregation assays were performed using 35 μM of substrate in 0.1 mL PBS (pH 7.4) at 35°C, denatured by 20 mM DTT, in both the presence and absence of CryAAID1-NP and indicated controls. Ins aggregation assays were performed using 75 μM of substrate in 0.1 mL PBS (pH 7.4) at 35°C, denatured by 20 mM DTT, in the presence and absence of CryAAID1-NP and indicated controls. Alpha-Lac aggregation assays were performed using 115 μM of substrate in 0.1 mL PBS (pH 7.4) at 35ºC, denatured by 20 mM DTT, in the presence and absence of CryAAID1-NP and indicated controls. All aggregation assays were performed in a clear bottom 96-well plate. Aggregation was monitored at 340 nm in a Molecular Devices M5e multi-mode plate reader under constant temperature (37°C), while shaking for 5 seconds between each read. All assays were

normalized based on the maximum absorbance of the averaged substrate (Lys, Ins, alpha-Lac) curves.

Chapter 2 References

1. Miao, Z.; Gao, Z.; Chen, R.; yu, X.; Su, Z.; Wei, G. *Surface-bioengineered Gold Nanoparticles for Biomedical Applications;* 2018; Vol. 25.
2. Arbach, H.; Butler, C.; McMenimen, K.,A. *Chaperone activity of human small heat shock protein-GST fusion proteins;* 2017; Vol. 22.
3. Makley, L. N.; McMenimen, K. A.; DeVree, B. T.; Goldman, J. W.; McGlasson, B. N.; Rajagopal, P.; Dunyak, B. M.; McQuade, T. J.; Thompson, A. D.; Sunahara, R. Pharmacological chaperone for α-crystallin partially restores transparency in cataract models. *Science* **2015***, 350*, 674-677.

CHAPTER 3 | RESULTS

3.1 | Chaperone Activity of B1NTR

The N-terminal region (NTR) of the human small heat shock protein (sHsp) HspB1 was isolated, purified, then characterized using SDS-PAGE gel electrophoresis and CD spectroscopy in preparation to analyze its ability to prevent aggregation of denatured model substrates in representation of its chaperone activity. HspB1NTR (residues 1-88) was produced through standard recombinant protein expression and purification. Purified HspB1NTR was shown to have a molecular weight of approximately 9.5 kDa (Figure 21C). CD spectroscopy was performed using soluble B1NTR at a concentration of 0.24 mg/mL to identify the presence of secondary structural elements. CD data was processed using two methods for comparison. The first, described by Raussens *et al.*, resulted in secondary structure identification of 6.5% beta-strand, 25.9% turn, 12.5% random, and 39.1% other structural elements.[1] The second method made use of CAPITO, as described by Wiedemann *et al.*[2] This method reported secondary structural elements of 26% helix, 13% beta-strand, and 61% irregular. The resulting CD spectroscopy trace overall showed a presence of alpha-helical secondary structure in addition to irregular secondary structural elements (Figure 21D).

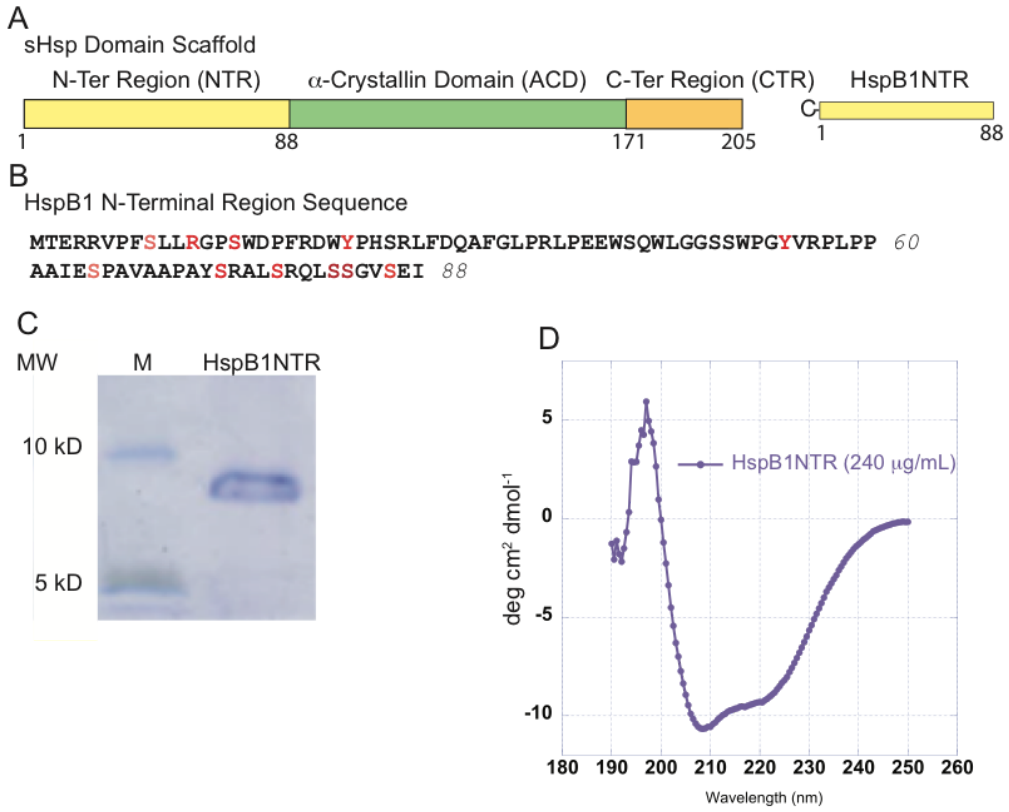

Figure 21. Domain organization, sequence, and characterization of HspB1NTR. (A) sHsps are defined by three regions, the N-terminal region (NTR), alpha-crystallin domain (ACD), and the C-terminal region (CTR). Residues 1-88 were isolated and defined as HspB1NTR. **(B)** The amino acid sequence of HspB1NTR. Residues highlighted in red undergo post-translational modifications. **(C)** SDS-PAGE gel of purified HspB1NTR. The protein marker (M) highlights standards at 5 kD (lowest band) and 10 kD (highest band) while HspB1NTR is ~9.5 kD. **(D)** CD spectroscopy of soluble HspB1NTR (0.24 mg/mL) at 25°C in 1x PBS, pH 7.4. Figure from Gliniewicz *et al*., 2019.[3]

Concentration-dependent changes in HspB1NTR were monitored using SEC and SDS-PAGE gel electrophoresis (Figure 22). Each sample was prepared using the same protein stock solution, diluted to the indicated concentrations (Figure 22A). At the lowest concentration of B1NTR tested (25 mM,

0.24mg/mL), a peak corresponding to large protein complexes was observed by SEC in addition to a monomer form, which was observed at approximately 9.5 kDa by SDS-PAGE (Figure 22). Peaks and corresponding gel fractions observed for 25 μM B1NTR indicate less protein relative to samples of B1NTR at higher concentrations (75 and 150 μM, 0.71 and 1.45 mg/ml, respectively). No shifting in peaks was observed in response to changing concentration (Figure 22A). The small peak eluting at approximately 21.5 mL likely corresponds to a minor contaminant (Figure 22A,B, lane D). At all three concentrations, a band was observed by SDS-PAGE at approximately 10 kDa, corresponding to B1NTR, though only the results of SDS-PAGE for 50 μM B1NTR are shown (Fig. 22B lanes B-C). Overall, B1NTR was seen to elute over a broad peak of approximately 2 mL. A standard curve was obtained for calibration of the gel filtration columns prior to evaluating B1NTR samples (Supplemental Information, Figure S1).

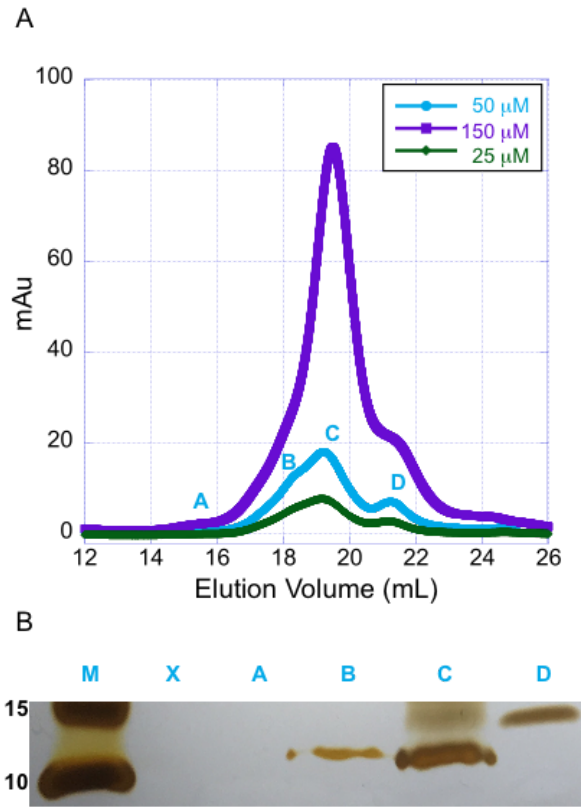

Figure 22. Concentration-dependent structural changes of soluble B1NTR. **(A)** Concentrations of soluble B1NTR at 25 μM (.21 mg/mL), 50 μM (.475 mg/mL), or 150 μM (1.47 mg/mL) were evaluated by SEC (Superose 6 10/30 increase) at 4°C. **(B)** Fractions collected from SEC evaluation (above) were identified by SDS-PAGE using silver stain of 50 μM (.475 mg/mL) B1NTR at 25°C. Fractions contributing to each peak were collected and combined prior to removing a sample for SDS-PAGE evaluation. Protein marker is indicated (M) and relative size is listed in kDa. X denotes a blank lane. Figure from Gliniewicz *et al*., 2019.[3]

The role of hydrophobic residues in the structure of B1NTR was analyzed using fluorescence changes in ANS binding before and after heating (Figure 23). A decrease in ANS fluorescence was observed as temperature increased from

25ºC to 45ºC, while little change occurred when the solution was heated further to 55ºC.

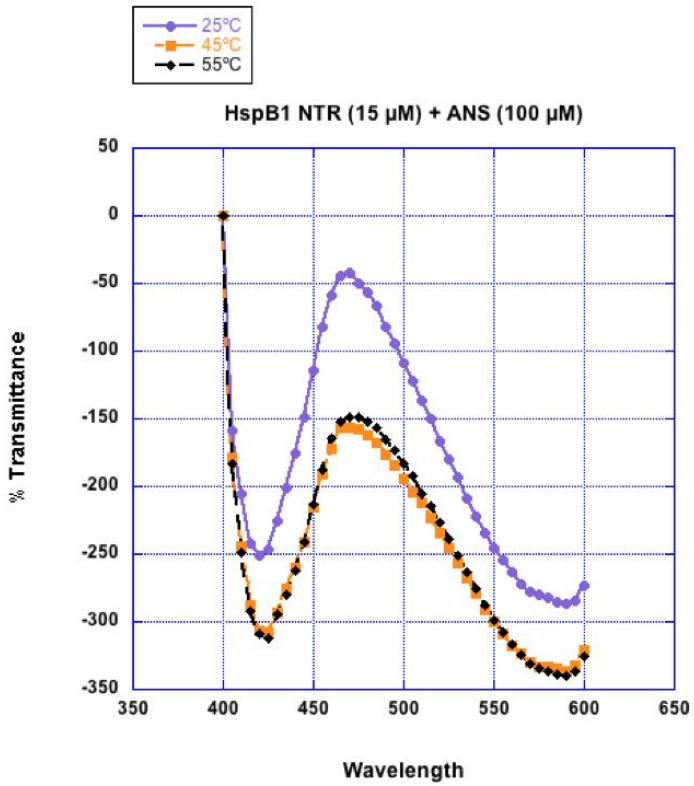

Figure 23. Temperature-dependent ANS binding to B1NTR. B1NTR (15 µM) and 1,8-ANS (100 µM) were mixed and incubated at 25°C, 45°C, 55°C for 1 hour before fluorescence readings were obtained. A decrease in ANS fluorescence was observed as temperature increased, indicating more ANS exchange with the solvent occurred upon heating. Figure from Gliniewicz *et al*., 2019.[3]

The *in vitro* chaperone activity of B1NTR was investigated using three model substrates. These results were compared to the chaperone activity of the full-length HspB1 on the same substrates. Heat-induced aggregation of MDH and CS, along with DTT-induced aggregation of Lys, were used to measure chaperone

activity. These substrates are widely used to measure chaperone activity, including that of other sHsps. Each denatured substrate has unique needs regarding chaperone concentration. Since the oligomerization of sHsps in solution is concentration dependent, as is the chaperone ability of sHsps on different substrates, several ratios of substrate to chaperone were tested. Control assays were performed to demonstrate the stability of B1NTR and the full-length HspB1 upon heating to 55ºC (Supplemental Information, Figure S2).

B1NTR was shown to exhibit a dose-dependent ability to suppress the aggregation of CS using light scattering measurements (Figure 24A). At a concentration ratio of 1:1, addition of B1NTR led to an increase in aggregation. Increasing the presence of B1NTR to a 1:6 (CS: B1NTR) ratio resulted in suppression of aggregation almost entirely, represented by the dramatic decrease in light scattering (Figure 24A). Comparing the chaperone activity of B1NTR on CS to that of the full-length chaperone, both at a 1:1 concentration ratio, indicates HspB1 has a greater chaperone activity on CS than does B1NTR, represented by lower levels of light scattering with addition of the former (Figure 24A). Addition of B1NTR at concentration ratios of 1:1 and 1:3 altered the lag phase as well as the overall aggregation of CS. An initial increase in aggregation was seen for lower concentrations of both B1NTR and HspB1 compared to that of the substrate in the absence of chaperone.

B1NTR was also shown to exhibit a dose-dependent suppression of aggregation for MDH and overall significant chaperone ability (Figure 24B). Comparing B1NTR and HspB1, both at 1:1 concentration ratios with MDH, B1NTR displayed more chaperone ability than full-length HspB1, as shown by a greater decrease in light scattering (Figure 24B). Both B1NTR and full-length HspB1 displayed a greater initial increase in aggregation than MDH alone. For both the full-length and NTR truncation, the lag phase of aggregation was altered compared to the aggregation of MDH in the absence of a chaperone. Compared to its chaperone capability on CS, B1NTR showed greater chaperone capability on MDH (Figure 24A,B).

To analyze the chaperone activity of B1NTR on substrates denatured in different ways, its activity on DTT-denatured Lys was characterized. B1NTR was shown to exhibit chaperone activity for Lys, where a 1:1 concentration ratio decreased substrate aggregation by approximately 50% (Figure 24C). Unlike the chaperone activity displayed with CS or MDH, the lag phase (representing the onset of aggregation) of Lys aggregation was unaffected by the presence of B1NTR. For Lys, B1NTR was shown to have better chaperone activity than full-length HspB1 (Figure 24C). Our data indicate, as exhibited by an increase in chaperone capacity of B1NTR for MDH and Lys relative to full-length HspB1, that substrate binding sites within B1NTR have chaperone activity.

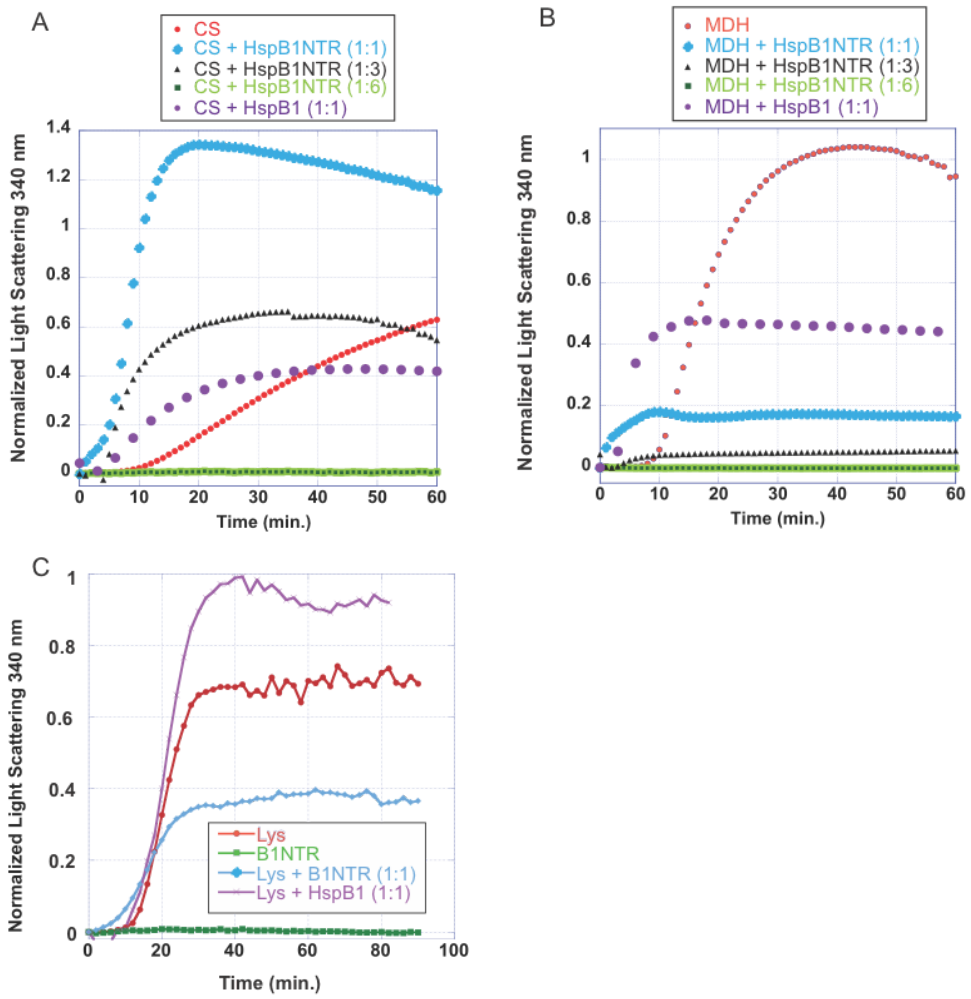

Figure 24. Aggregation of denatured substrate proteins CS, MDH, and Lys in the presence of B1NTR and wild-type HspB1. (A) Heat-induced CS (2.5 μM) aggregation in the presence of 2.5, 7.5, or 15 μM B1NTR or wild-type HspB1 (2.5 μM) at 45°C. **(B)** Heat-induced MDH (15 μM) aggregation in the presence of 2.5, 7.5, or 15 μM B1NTR or wild-type HspB1 (2.5 μM) at 45°C. **(C)** DTT-induced (20 mM) aggregation of Lys (35 μM) in the presence of B1NTR (35 μM) or wild-type HspB1 (35 μM) at 37°C. Each curve is an average of ≥ 4 independent replicates. Data was normalized to the maximum absorbance of the averaged respective substrate curves. Figure from Gliniewicz *et al*., 2019.[3]

3.2 | Size Exclusion Chromatography of Substrate-Chaperone Complexes

To determine whether B1NTR forms complexes with its substrate in solution, mixtures of B1NTR and each of the three model substrates were analyzed with SEC and SDS-PAGE gel electrophoresis. Mixtures of chaperone and substrate were incubated for 1 to 3 hours at 45ºC and the distribution of species was compared to each unmixed sample (Figure 25). Samples containing 1:1 mixtures of B1NTR and MDH or Lys were allowed to incubate for an hour under heat- and chemical-denaturing conditions, respectively, then were evaluated by SEC and SDS-PAGE (Figure 25A-D). The mixture containing a 1:1 concentration ratio of Lys to B1NTR resulted in SEC shifts to smaller elution volumes and peaks with more distinct form relative to Lys alone (Figure 25A). SDS-PAGE analysis of SEC fractions indicate that B1NTR and Lys co-elute (Figure 25A,B).

Similar analysis of a mixture of 1:1 concentration ratio of MDH to B1NTR resulted in shifts toward larger elution volumes with broader peaks, indicating a change in hydrodynamic radius of the protein mixture relative to each substrate or chaperone run alone (Fig. 25C, D). Peaks 2 and 3 shifted to larger elution volumes relative to MDH (peaks 4-6) and B1NTR alone, corresponding to a longer retention time and a protein complex with a smaller hydrodynamic radius. SDS-PAGE analysis of peak fractions resulted in a broad band distribution, indicating MDH and B1NTR elute together (Figure 25D). It should

be noted that although MDH was purchased from a supplier and indicated to be pure, both the SEC and SDS-PAGE data indicate likely contamination (Figure 25C, D).

SEC analysis of the interaction between B1NTR and CS at a concentration ratio of 10 to 1 indicated some complex formation occurs with a large excess of chaperone to substrate, however no chaperone activity was observed when less chaperone was present (Figure 25E, Supplemental Information Figure S3). At a 10:1 ratio, B1NTR and CS co-elute over a broad range. Similar to MDH, CS also exhibited impurities as observed by SDS-PAGE (Figure 25F).

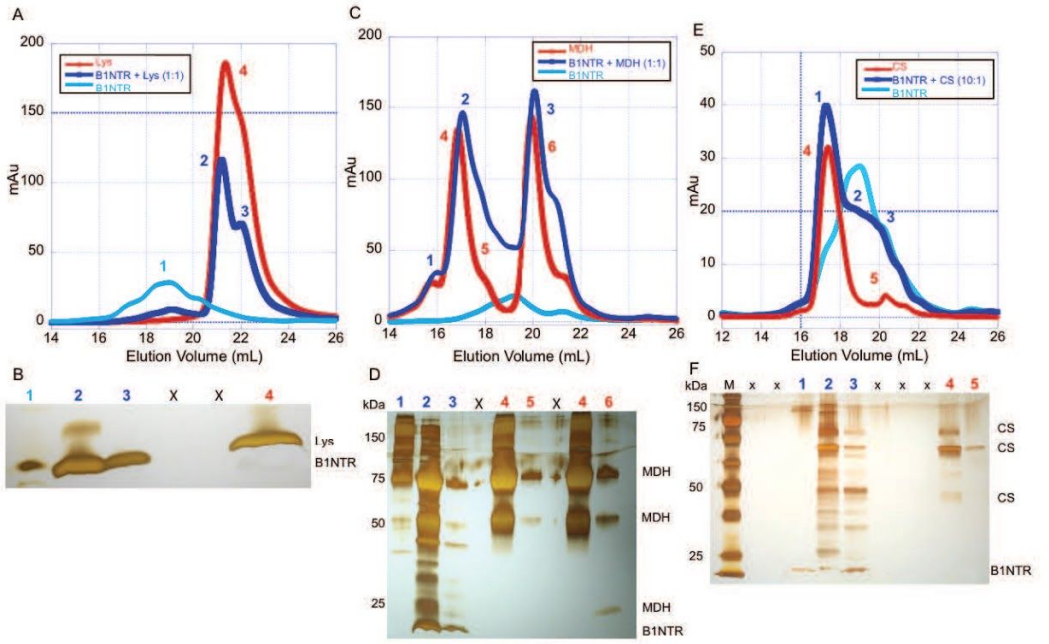

Figure 25. B1NTR forms complexes with substrates during protein aggregation. (A) After incubation for 1 hr at 45°C with 20mM DTT, mixed samples of (1:1) Lys (75 μM) and B1NTR (75 μM) or each protein individually, were evaluated by SEC on a Superose 6 10/30 increase column at 0.3 mL/min. Peak fractions are indicated by numbers. **(B)** SDS-PAGE gel of respective sample elution fractions corresponding to observed peaks. Protein molecular mass marker is in far-left lane. Each indicated gel lane represents a sample taken from a fraction corresponding to those indicated on SEC traces, above. 1: B1NTR only, 2: B1NTR + Lys, 3: B1NTR + Lys, X: spillover lanes, 4: Lys only. **(C)** Mixed samples (1:1) B1NTR (50 μM) and MDH (50 μM) were evaluated by SEC after heating at 45°C for 1 hr. Individual samples were obtained under similar conditions. Peak fractions are indicated by numbers. **(D)** SDS-PAGE gel of each respective peak elution obtained from independent SEC runs. Each indicated gel lane represents a peak obtained from multiple fractions and labeled on corresponding SEC traces, above. **(E)** A 10:1 ratio of B1NTR (50 μM) and CS (5 μM) was evaluated by SEC after heating at 45°C for 1 hr. Individual sample evaluations were obtained under similar conditions. Peak fractions are indicated by numbers. **(F)** SDS-PAGE gel of each respective peak elution obtained from independent SEC runs. Each indicated gel lane represents a peak obtained from multiple fractions and is labeled on corresponding SEC trace in (E). M: protein molecular weight marker, X: spillover lanes, 1: B1NTR + CS, 2: B1NTR + CS, 3: B1NTR + CS, 4: CS only, 5: CS only. Figure from Gliniewicz *et al*., 2019.[3]

3.3 | Chaperone Activity of B1NTR-Conjugated Nanoparticles

To determine whether the immobilization of B1NTR to gold nanoparticles and its subsequent increase in local concentration resulted in active chaperone peptides, B1NTR-AuNPs were produced by coupling purified B1NTR to 5 nm and 10 nm AuNPs coated with NHS-terminated PEG linkers. PEG linkers were inserted between the AuNP surface and the peptide to reduce potential non-specific interactions between citrate-stabilized AuNPs (unconjugated) and denaturing substrates. The resulting B1NTR-AuNPs (B1NTR-NPs) were coated with ≥ 10 B1NTR peptides per AuNP and exhibited increased diameters, as well as altered zeta-potentials after coupling (Supplemental Information, Figure S4, Table S1). The chaperone activity of B1NTR-NPs was evaluated using three model substrate proteins. In addition, the effect of nanoparticle size on the chaperone capacity of B1NTR-NPs was examined using the substrate protein Lys and comparing 5 nm and 10 nm NP conjugates.

B1NTR-NPs (10 nm) exhibited dose-dependent suppression of heat-induced CS aggregation (Figure 26A). At the lowest concentration of B1NTR-NP tested (14.9 nM), only a slight shift in aggregation was observed compared to CS alone. At higher concentrations of B1NTR-NP (29.9 nM), CS aggregation was suppressed by approximately 50%. In contrast to the results observed for unconjugated B1NTR, the B1NTR-NPs did not alter the lag phase of CS aggregation. B1NTR-NPs also exhibited dose-dependent suppression of

aggregation for the substrate protein MDH, with trends in agreement with data obtained using unconjugated B1NTR. At the highest concentration of B1NTR-NP (29.9 nM), its chaperone capacity prevented approximately 70% of MDH aggregation. In contrast to the results with CS, even very low concentrations of B1NTR-NP (7.5 nM) were able to suppress MDH aggregation (Figure 26A,B). In the presence of B1NTR-AuNPs the lag phase during MDH aggregation increased slightly, which contrasts its decrease observed when unconjugated B1NTR was used. Next, the solubility of B1NTR-NP complexes with CS and MDH were evaluated using SDS-PAGE to determine the proteins present in soluble and insoluble fractions (Figure 26C,D). Increasing concentrations of B1NTR-NP produced slight decreases in the amount of insoluble substrate for both CS and MDH. MDH-B1NTR and MDH-B1NTR-AuNP complexes were observed by TEM (Supplemental Information, Figure S5). TEM results showed a reduction in larger protein aggregates in both chaperone-containing mixtures compared to MDH only samples, consistent with solution-phase data.

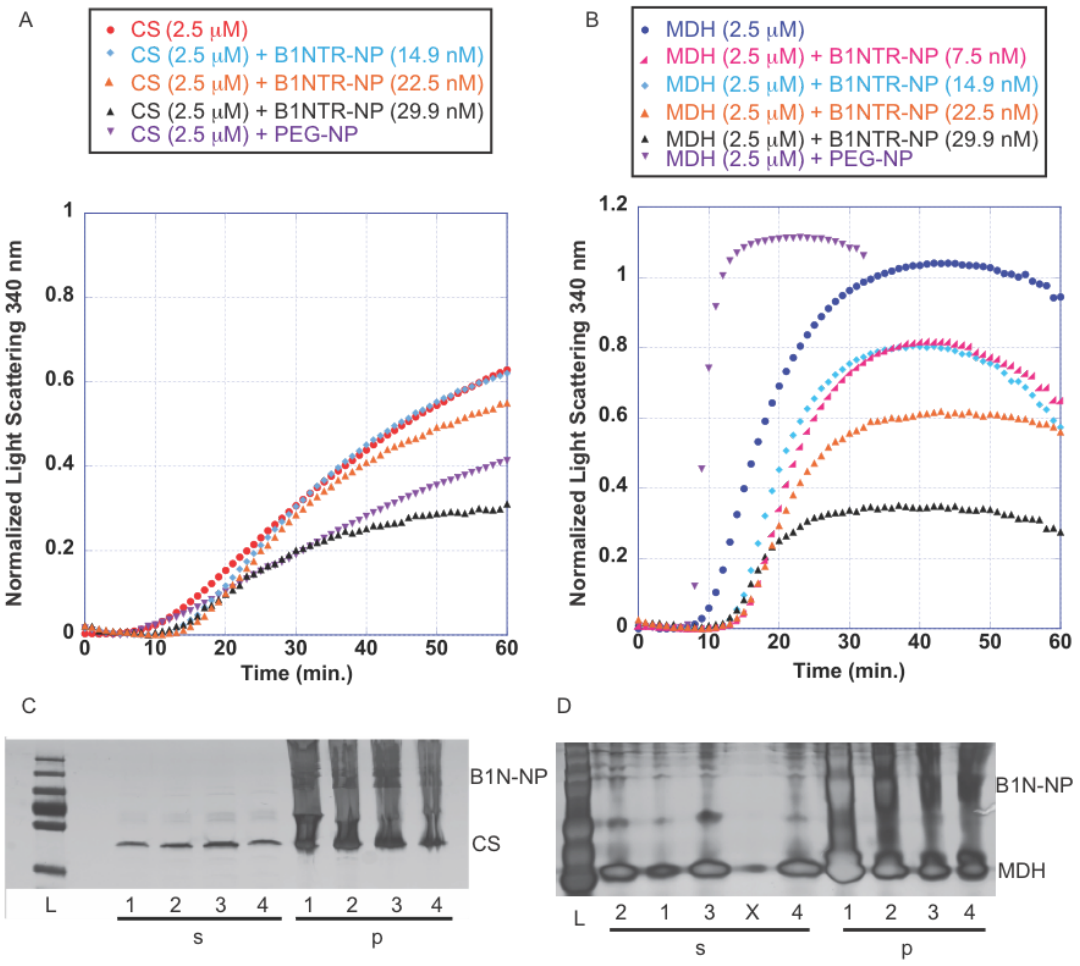

Figure 26. Chaperone-like activity during heat-induced aggregation of substrates CS and MDH. (A) Heat-induced CS (2.5 μM) aggregation in the presence of 14.9, 22.5, 29.9 nM B1NTR-NP or PEG-NP (7.48 nM) at 45°C. **(B)** Heat-induced MDH aggregation in the presence of 7.5, 14.9, 22.5, 29.9 nM B1NTR-NP or PEG-NP (7.48 nM) at 45°C. Each curve is an average of ≥ 3 replicates. **(C)** Mixed samples of CS (2.5 μM) and B1NTR-NP were separated into soluble (s) and insoluble (p) fractions and analyzed by SDS-PAGE after shaking for 1 hr at 45°C. Samples are L: Molecular mass marker, 1: CS only, 2: CS + B1NTR-NP (14.9 nM), 3: CS + B1NTR-NP (22.5 nM), 4: CS + B1NTR-NP (29.9 nM). **(D)** Mixed samples of MDH (2.5 μM) and B1NTR-NP were separated into soluble (s) and insoluble (p) fractions and analyzed by SDS-PAGE after shaking for 1 hr at 45°C. Samples are L: Molecular mass marker, 1: MDH only, 2: MDH + B1NTR-NP (7.5 nM), 3: MDH + B1NTR-NP (14.8), X: spillover lane, 4: MDH + B1NTR-NR (29.9 nM). All SDS-PAGE gels were developed using silver staining. Results displayed in this figure obtained by Diana Sibai. Figure from Gliniewicz *et al.*, 2019.[3]

To exclude the possibility that the PEG linker was responsible for results suggesting B1NTR-NP chaperone activity, methyl-terminated PEG-AuNPs were tested with all three model substrates. These PEG linkers attached to the gold nanoparticles have a methyl group terminating their free ends in place of B1NTR (Figures 26A,B, 27B). The specific result of the interaction, either an observed increase or decrease in aggregation, is substrate-dependent, since the presence of PEG-NPs decreased aggregation of CS and Lys, but increased aggregation of MDH.

B1NTR-NPs were evaluated in the presence of Lys, which undergoes DTT-induced substrate denaturation, to evaluate the effects of substrate denaturation conditions on their chaperone activity. Additionally, the influence of AuNP size on chaperone capacity was evaluated by immobilizing B1NTR to 5 nm and 10 nm PEG-AuNPs. Soluble B1NTR displayed chaperone activity for Lys at a concentration ratio of 1:2.3 (Figure 27A). When B1NTR was conjugated to 10 nm AuNPs, there was a decrease in the observed lag time of initial substrate aggregation, as well as an increase in overall substrate aggregation in the presence of more concentrated B1NTR-AuNP samples (Figure 27B). Some, yet relatively little, chaperone activity was observed for more dilute B1NTR-AuNP samples. When 5 nm B1NTR-AuNPs were evaluated under the same conditions, a dose-dependent decrease in aggregation of Lys was observed, along with an increase in the lag phase (Figure 27C). The aggregation of Lys in the presence of

unconjugated AuNPs (5 and 10 nm) was evaluated as a control, and showed no dose-dependent chaperone activity (Supplemental Information, Figure S6).

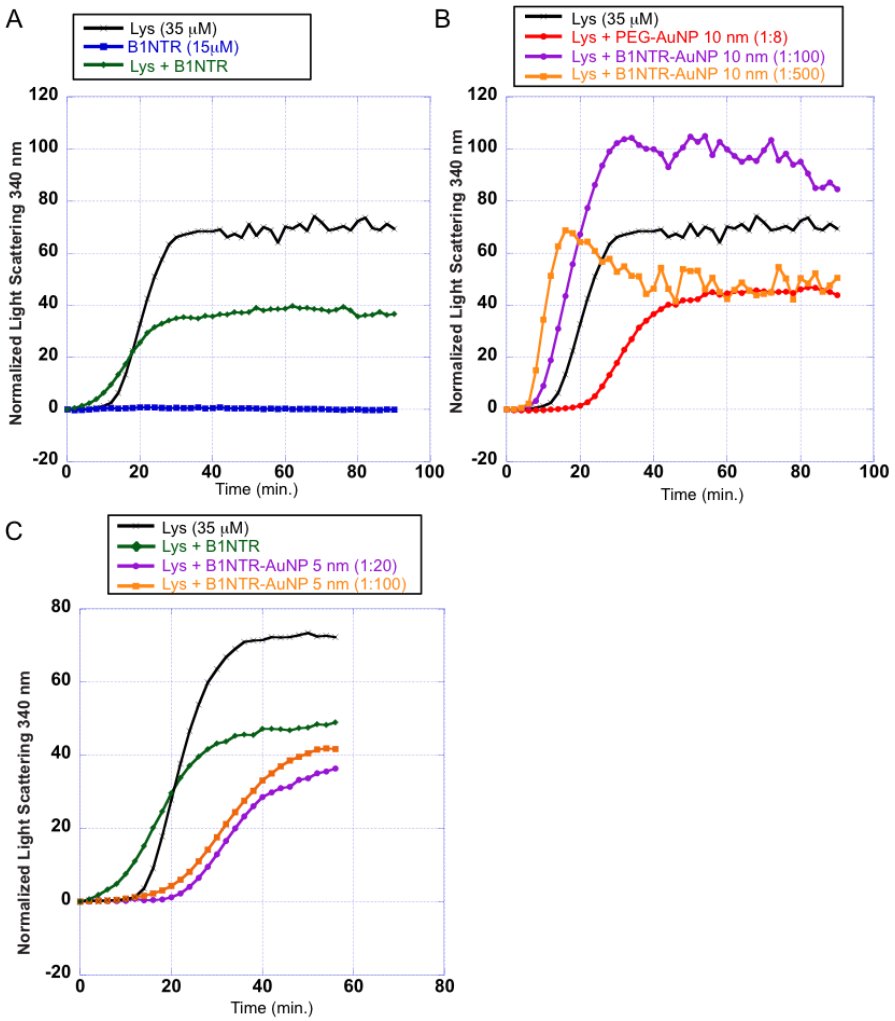

Figure 27. Chemically induced aggregation of denatured Lys (35 μM) by DTT (20 mM) in the presence and absence of conjugated B1NTR-AuNPs. (A) Chemically-induced aggregation of 35 μM Lys (black), Lys (35 μM) in presence of 15 μM B1NTR (green), and 15 μM B1NTR only (blue) with DTT (20 mM) at 37°C. **(B)** Aggregation of Lys (35 μM) by DTT (20 mM) at 37°C in the presence of 10 nm conjugated B1NTR-AuNPs (OD 10) at dilutions 1:100 and 1:500 (final concentration), and 10 nm PEG-AuNP (1:8 dilution). All dilutions are calculated relative to the initial concentration of OD 10 for each 10 nm AuNP sample. All dilutions performed in 1x PBS, pH 7.4 **(C)** Chemically-induced aggregation of Lys (35 μM) with DTT (20 mM) at 37°C in the presence of 5 nm B1NTR-AuNPs (OD 2) at final dilutions of 1:20 (purple) and 1:100 (orange) relative to starting OD 2 for each AuNP sample. Each curve is the average of ≥ 3 independent trials. Results in this figure obtained by Diana Sibai. Figure from Gliniewicz *et al.*, 2019.[3]

3.4 | Chaperone Activity of CryAAID1-Conjugated Nanoparticles

The studies above were performed with the entire (88 residue) HspB1NTR to evaluate its activity in solution and conjugated to nanoparticles. Due to its activity, we were interested in further studies to try to evaluate smaller regions of activity within the N-terminal domain that may exhibit chaperone capacity. The following studies utilized a much smaller peptide (18 residues long) from within the NTR of human sHsp alpha-crystallin A (HspB4) to evaluate its chaperone capacity and characterize its function. One of our goals was to identify binding regions within the sHsp that specifically interact with different substrates to facilitate a "map" of protein-protein interacting regions.

To characterize the *in vitro* chaperone activity of CryAAID1 (residues 70-88 of alpha-crystallin A), its capability to suppress the DTT-induced aggregation of Lys was evaluated (Figure 28A). Both 35 μM and 70 μM CryAAID1 displayed overall chaperone activity, although not in a dose-dependent manner. The more concentrated sample of CryAAID1 did, however, display an increase in the lag phase, while the less concentrated sample did not, suggesting altered aggregation behavior of the substrate. To determine whether the immobilization of the CryAAID1 peptide on to AuNPs affected its chaperone abilities, it was conjugated to 10 nm AuNPs coated with NHS-terminated PEG linkers, as described above in use with B1NTR. While dilute samples of CryAAID1-AuNPs displayed no chaperone activity (1:100) or even an increase in

aggregation (1:200), higher concentrations showed a dose-dependent ability to suppress Lys aggregation (Figure 28B). As explained for use with B1NTR, methyl-terminated PEG coated NPs were used as a control and some non-specific interactions with Lys were observed.

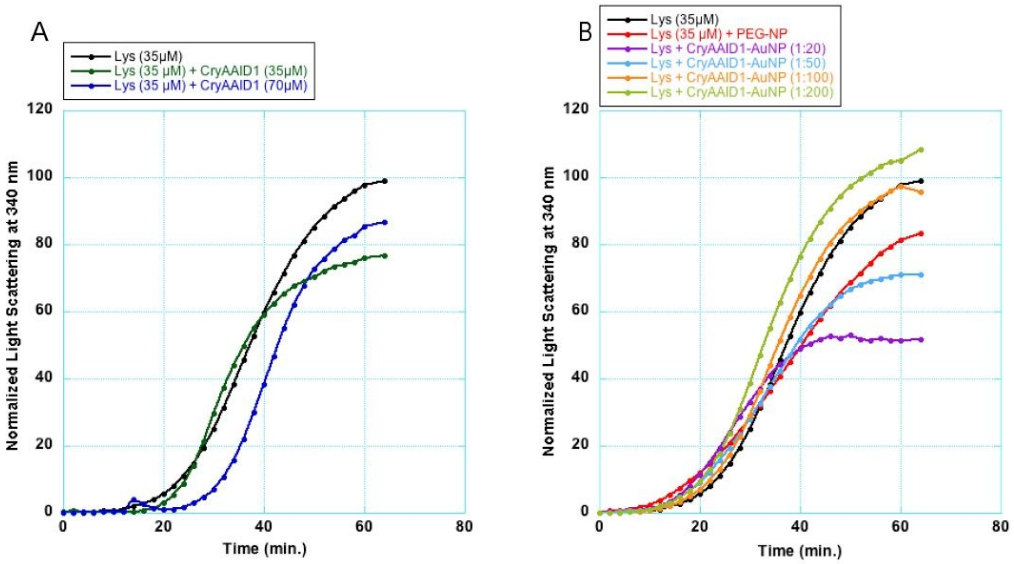

Figure 28. Chemically induced aggregation of denatured Lys (35 µM) by DTT (20 mM) in the presence and absence of 10 nm conjugated CryAAID1-AuNPs. (A) Chemically-induced aggregation of 35 µM Lys (black), Lys (35 µM) in presence of 35 µM CryAAID1 (green), and Lys (35 µM) in the presence of 70 µM CryAAID1 (blue) with DTT (20 mM) at 35°C. **(B)** Aggregation of Lys (35 µM) by DTT (20 mM) at 35°C in the presence of 10 nm conjugated CryAAID1-AuNPs (OD 1) at dilutions 1:20, 1:50, 1:100 and 1:200 (final concentration) of sHsp-AuNP, and 10 nm PEG-AuNP. All dilutions are calculated relative to the initial concentration of OD 1 for each 10 nm AuNP sample. All dilutions performed in 1x PBS, pH 7.4. Assay optimized by fellow undergraduate Helen C. Campbell.

To examine the effect of nanoparticle size on the chaperone capacity of CryAAID1-AuNPs, the above experiments were repeated with 5 nm CryAAID1-AuNPs. Overall, 5 nm CryAAID1-AuNPs displayed minimal chaperone activity, which was comparatively less than 10 nm CryAAID1-AuNPs at both 1:50 and 1:20 concentration ratios (Figures 28B, 29B). Since CryAAID1-AuNPs began to show a minimal increase in chaperone activity at a ratio of 1:20, higher concentrations were tested (Figure 29A). With higher concentrations, there was a slight dose-dependent trend of chaperone activity for 1:20 and 1:10, with no effect on the lag phase. Interestingly, the 1:5 concentration ratio displayed an increase in the lag phase and an overall decrease in time taken to reach maximum aggregation, peaking sooner than Lys alone, and at almost the same light scattering intensity.

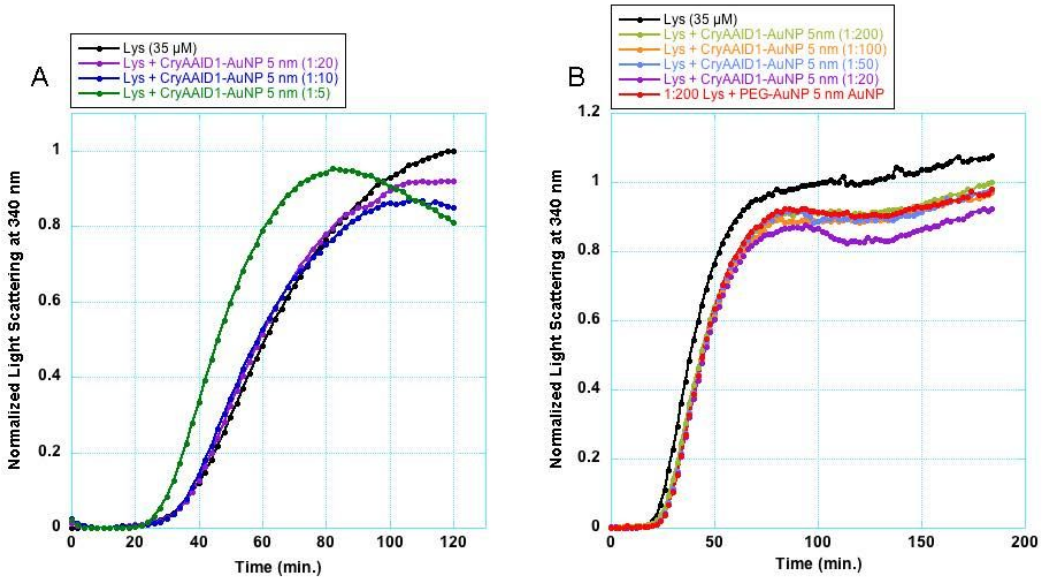

Figure 29. Chemically induced aggregation of denatured Lys (35 µM) by DTT (20 mM) in the presence and absence of 5 nm conjugated CryAAID1-AuNPs. (A) Characterization of chaperone-like activity of CryAAID1-AuNPs at high concentrations. Chemically-induced aggregation of 35 µM Lys (black) and of Lys (35 µM) in the presence of 5 nm conjugated CryAAID1-AuNPs (OD 1) at dilutions 1:20, 1:10, and 1:5 (final concentration) with DTT (20 mM) at 35°C. **(B)** Aggregation of Lys (35 µM) by DTT (20 mM) at 35°C in the presence of 5 nm conjugated CryAAID1-AuNPs (OD 1) at dilutions 1:200, 1:100, 1:50 and 1:20 (final concentration), and 5 nm PEG-AuNP (1:200 dilution). All dilutions are calculated relative to the initial concentration of OD 1 for each 5 nm AuNP sample. All dilutions performed in 1x PBS, pH 7.4.

Another common model substrate, Insulin (Ins) was tested to evaluate substrate specificity of both the free CryAAID1 peptide and CryAAID1-AuNPs. The DTT-induced aggregation of Ins (75 µM) was suppressed by CryAAID1 (50 µM) by approximately 50%, a significant display of chaperone ability in comparison to the results for Lys (Figure 30A). Additionally, the presence of CryAAID1 caused an increase in the lag phase. Next, 10 nm CryAAID1-AuNPs

were evaluated and displayed an overall dose-dependent suppression of the aggregation of Ins, with no significant effect on the lag phase (Figure 30B).

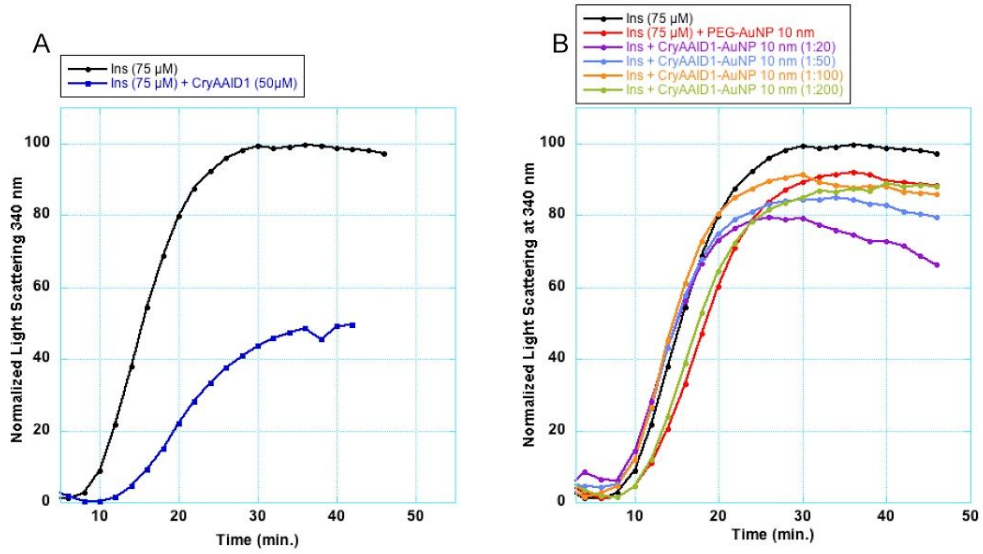

Figure 30. Chemically induced aggregation of denatured Ins (75 µM) by DTT (20 mM) in the presence and absence of 10 nm conjugated CryAAID1-AuNPs. (A) Chemically-induced aggregation of 75 µM Ins (black) and of Ins (75 µM) in the presence of CryAAID1 (50 µM) with DTT (20 mM) at 35°C. **(B)** Aggregation of Ins (75 µM) by DTT (20 mM) at 35°C in the presence of 10 nm conjugated CryAAID1-AuNPs (OD 1) at dilutions 1:20, 1:50, 1:100 and 1:200 (final concentration), and 10 nm PEG-AuNP. All dilutions are calculated relative to the initial concentration of OD 1 for each 10 nm AuNP sample. All dilutions performed in 1x PBS, pH 7.4. Assay optimized by fellow undergraduate Helen C. Campbell.

To determine the effect of nanoparticle size on the chaperone activity of CryAAID1-AuNP for Ins, the above experiments were repeated with 5 nm CryAAID1-AuNPs. These conjugates showed little-to-no chaperone activity (Figure 31A). Though enlargement of the results shows slight differences, they

are likely insignificant interactions (Figure 31B). This interpretation is supported by the appearance of 5 nm PEG-AuNPs to exhibit the lowest level of light scattering and therefore the least amount of Ins aggregation. All concentrations tested displayed aggregation suppression of less than 10%. None of the 5 nm CryAAID1-AuNP samples affected the lag phase of Ins aggregation.

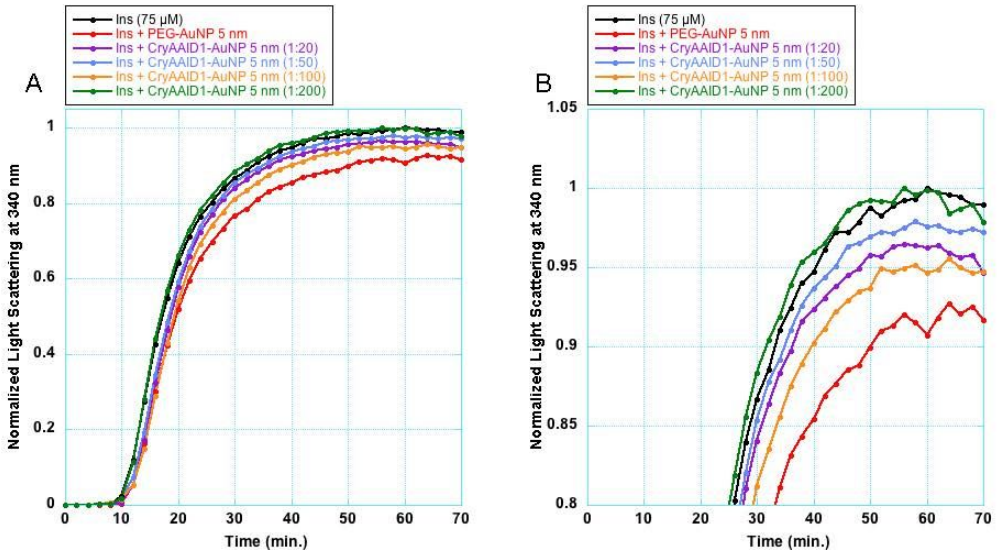

Figure 31. Chemically induced aggregation of denatured Ins (75 µM) by DTT (20 mM) in the presence and absence of 5 nm conjugated CryAAID1-AuNPs. **(A)** Chemically-induced aggregation of 75 µM Ins (black) and of Ins (75 µM) in the presence of 5 nm conjugated CryAAID1-AuNPs (OD 1) at dilutions 1:20, 1:50, 1:100, 1:200 (final concentration), and 5 nm PEG-AuNP (1:200 dilution) with DTT (20 mM) at 35°C. All dilutions are calculated relative to the initial concentration of OD 1 for each 5 nm AuNP sample. All dilutions performed in 1x PBS, pH 7.4. **(B)** Enlargement of upper portion of (A) to show clearer separation between aggregation levels of different CryAAID1-AuNP dilutions.

Since CryAAID1, both free and conjugated to NPs, displayed quite different chaperone activity between the two substrates tested above, the

characterization of its substrate specificity was continued with the analysis of DTT-induced aggregation of alpha-Lactalbumin (alpha-Lac). The aggregation of alpha-Lac (115 µM) was suppressed approximately 25%, accompanied by an increase in the lag phase, in the presence of free CryAAID1 peptide at a concentration of 60 µM (Figure 32A). 10 nm CryAAID1-AuNPs displayed chaperone activity for alpha-Lac at all tested concentrations, though not in a dose-dependent manner. An increase in lag phase was seen in varying degrees for all CryAAID1-AuNP samples. Interestingly, 10 nm PEG-AuNPs displayed the largest increase in the lag phase.

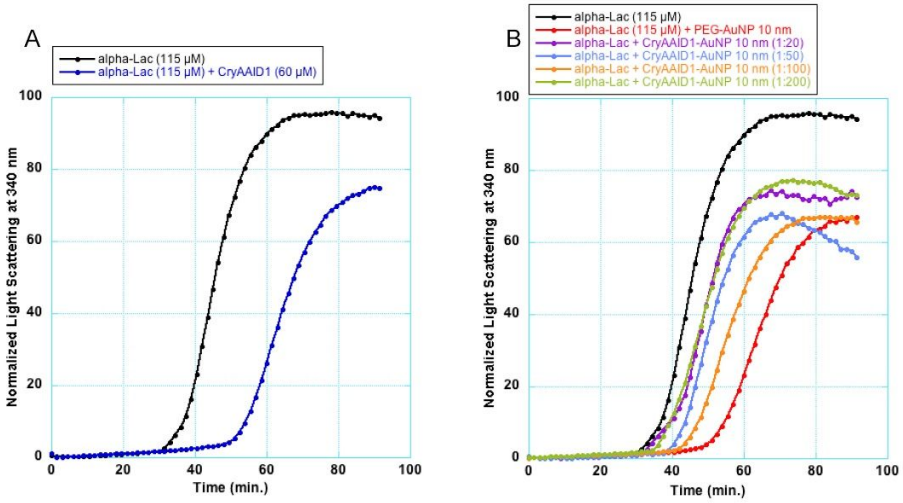

Figure 32. Chemically-induced aggregation of denatured alpha-Lac (115 µM) in the presence and absence of 10 nm conjugated CryAAID1-AuNPs. (A) Chemically-induced aggregation of 115 µM alpha-Lac (black), alpha-Lac (115 µM) in presence of 80 µM CryAAID1 (blue) with DTT (20 mM) at 35°C. **(B)** Aggregation of alpha-Lac (115 µM) by DTT (20 mM) at 35°C in the presence of 10 nm conjugated CryAAID1-AuNPs (OD 1) at dilutions 1:20, 1:50, 1:100, 1:200 (final concentration), and 10 nm PEG-AuNP (1:200 dilution). All dilutions are calculated relative to the initial concentration of OD 1 for each 10 nm AuNP sample. All dilutions performed in 1x PBS, pH 7.4. Assay optimized by fellow undergraduate Helen C. Campbell.

When the effect of nanoparticle size on CryAAID1-AuNP chaperone activity was tested, 5 nm CryAAID1-AuNPs displayed little-to-no ability to suppress the DTT-induced aggregation of alpha-Lac (Figure 33). Interestingly, alpha-Lac alone demonstrated a brief plateau before rapidly increasing, suggesting the formation of an intermediate during aggregation. Addition of 5 nm CryAAID1-AuNPs eliminated the appearance of this intermediate, but did not significantly reduce aggregation of the substrate. The presence of 5 nm PEG-NPs actually displayed a larger, but still slight, overall decrease in alpha-Lac aggregation. Effects of both PEG-AuNPs and CryAAID1-AuNPs of 5 nm did not appear to be concentration dependent.

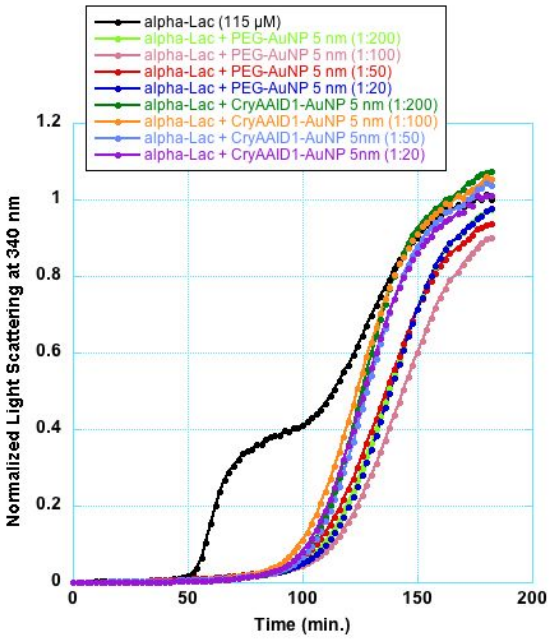

Figure 33. Chemically induced aggregation of denatured alpha-Lac (115 µM) by DTT (20 mM) in the presence and absence of 5 nm conjugated CryAAID1-AuNPs. (A) Chemically-induced aggregation of 115 µM alpha-Lac (black) and of alpha-Lac (115 µM) in the presence of 5 nm conjugated CryAAID1-AuNPs (OD 1) at dilutions 1:200, 1:100, 1:50, and 1:20 (final concentration), and with PEG-AuNPs at dilutions 1:200, 1:100, 1:50, and 1:20, by DTT (20 mM) at 35°C. All dilutions are calculated relative to the initial concentration of OD 1 for each 5 nm AuNP sample. All dilutions performed in 1x PBS, pH 7.4.

Chapter 3 References

1. Raussens, V.; Ruysschaert, J.; Goormaghtigh, E. Protein concentration is not an absolute prerequisite for the determination of secondary structure from circular dichroism spectra: a new scaling method. *Anal. Biochem.* **2003***, 319*, 114-121.
2. Wiedemann, C.; Bellstedt, P.; Görlach, M. CAPITO—a web server-based analysis and plotting tool for circular dichroism data. *Bioinformatics* **2013***, 29*, 1750-1757.
3. Gliniewicz, E. F.; Chambers, K. M.; De Leon, E. R.; Sibai, D.; Campbell, H. C.; McMenimen, K. A. Chaperone‐like activity of the N‐terminal region of a human small heat shock protein and chaperone‐functionalized nanoparticles. *Proteins: Structure, Function, and Bioinformatics* **2019**.

CHAPTER 4 | DISCUSSION

4.1 | Characterization of B1NTR Structure

sHsp NTRs are generally considered to have relatively few secondary or other structural elements. There are likely multiple three-dimensional conformations of the NTR that can contribute to the structure of the sHsp as a whole, and these conformations are likely influenced by factors such as concentration, substrates, and post-translational modifications.[1] CD spectroscopy analysis of B1NTR indicated its secondary structure, in addition to irregular or unstructured elements, was primarily alpha-helical, which had not yet been determined (Figure 21D). SEC analysis of B1NTR indicated the presence of both monomers and large protein complexes. The lack of any shifting in peaks between samples differing in concentration suggests the level of sHsp oligomerization is not dependent on its concentration in solution (Figure 22). The broadness of the elution peak for B1NTR likely arose from its variety of conformations. The decrease in ANS fluorescence with increasing temperature suggests hydrophobic residues within the NTR become increasingly exposed in solution as temperature rises (Figure 23). It is possible that B1NTR has exposed hydrophobic regions in solution due to some unstructured features, especially at lower concentrations where sHsp oligomers may not be present.

4.2 | Chaperone Activity of B1NTR

The *in vitro* chaperone activity of B1NTR was tested against full-length HspB1 on three model substrates: MDH, CS, and Lys. Using multiple substrates, the first two of which are heat denatured and a third that is DTT-denatured, allowed the evaluation of B1NTR's chaperone activity on a wide range of substrates. The use of different concentrations of B1NTR enabled the identification of concentration-dependent differences in sHsp oligomer formation, as well as the amount of B1NTR necessary to perform chaperone activity on different substrates. With CS as its substrate, B1NTR exhibited dose-dependent suppression of aggregation, but appeared less active than full-length HspB1 (Figure 24A). Greater chaperone capability of full-length HspB1 is likely attributed to the presence of more than one substrate binding site outside of the NTR, as well as the ability of the full-length sHsp to form more oligomeric states. The increase in aggregation of CS in the presence of a low concentration of B1NTR suggests that B1NTR is interacting with CS early on in unfolding and is co-aggregating with the substrate. Significant chaperone activity without an initial increase in aggregation isn't seen until the concentration ratio of 1:6 substrate to B1NTR. Full-length B1NTR also exhibited an initial increase in aggregation, though its overall chaperone capacity was higher than that of B1NTR. Perhaps the ACD or CTR of HspB1 is required along with the NTR to maintain chaperone activity.

B1NTR was seen to suppress the aggregation of MDH in a dose-dependent manner and with significant chaperone activity, in this case more than full-length HspB1 (Figure 24B). There was an initial increase in MDH aggregation for low concentrations (1:1) of both B1NTR and full-length HspB1. A decrease in the lag phase of MDH aggregation suggests B1NTR, as well as full-length HspB1, may interact with MDH during unfolding and change its unfolding pathway relative to that exhibited in the absence of a chaperone. The greater chaperone activity of B1NTR on MDH compared to that of full-length HspB1 may be attributed to increased efficiency of interactions between the substrate and B1NTR. This may indicate that within the full-length sHsp, the NTR contributes to the regulation of sHsp-substrate binding. Perhaps the presence of the ACD and CTR decreases substrate-chaperone interactions, or at least early association between the NTR and substrate. This regulatory effect of the full-length sHsp may be physiologically important in times of cellular stress to control time, location, and level of substrate-chaperone interactions. Furthermore, the difference in chaperone activity of B1NTR on MDH compared to CS is evidence that B1NTR has substrate specificity, and does not bind all substrates equally *in vitro*.

Using Lys as a model substrate allowed for consideration of a substrate's mode of denaturation and its role in substrate-sHsp interactions. B1NTR exhibited overall chaperone activity for Lys, in a way similar to MDH, except B1NTR did

not alter the lag phase of Lys aggregation (Figure 24C). This indicates B1NTR had little to no effect on Lys unfolding, and acted only to prevent further aggregation of already dentured Lys. Differences in B1NTR chaperone activity on Lys may be attributed to its different mechanism of unfolding compared to that of CS and MDH. Similarly to MDH, B1NTR exhibited stronger chaperone activity for Lys than did full-length HspB1. These results suggest that controlled oligomeric dynamics in full-length HspB1 may reduce sHsp activity in a substrate-specific manner, which B1NTR is lacking. The fact that B1NTR has less quaternary structure and demonstrates more chaperone capacity for some substrates suggests that the availability of the NTR for interactions with Lys is essential to chaperone activity. The increase in chaperone capacity of B1NTR for MDH and Lys relative to full-length HspB1 suggests that substrate binding sites within B1NTR have chaperone activity and act on some, but not all substrates.

4.3 | Size-Exclusion Chromatography of Substrate-Chaperone Complexes

B1NTR and its interactions with model substrates were analyzed by SEC to evaluate the formation of complexes between them in solution. Co-elution of substrate and chaperone indicates formation of complexes. The SEC analysis of a mixture of equimolar B1NTR and Lys resulted in more distinct peaks shifted to smaller elution volumes, suggesting complex formation occurs in a homogenous sample (Figure 25A). Because the co-elution peak (labeled ‘2’ in Figure 25A) is

seen at a larger elution volume than B1NTR alone, this suggests the formed complex is more compact that either protein alone.

SEC results of an equimolar mixture of B1NTR and MDH exhibited broadened peaks shifted to slightly larger elution volumes relative to B1NTR alone, corresponding to a longer retention time and a smaller hydrodynamic radius (Figure 25C). SDS-PAGE results confirmed co-elution of MDH and B1NTR. Although the change is subtle, these results suggest substrate-chaperone complexes of B1NTR and MDH are sufficient to alter SEC distribution of the proteins in the mixture.

SEC analysis of interactions between B1NTR and CS required a 10:1 concentration ratio of B1NTR to CS for observable complex formation to occur. With B1NTR in large excess, the two components co-elute over a broad range, suggesting several different complexes may be present (Figure 25E). Under these conditions, the chaperone likely prevented CS aggregation simply by disrupting CS-CS interactions. It is also possible that the impurities present in CS are able to interact with B1NTR and may contribute to the broad peak of SEC co-elution.

4.4 | Chaperone Activity of B1NTR-Conjugated Nanoparticles

B1NTR was conjugated to 5 and 10 nm gold nanoparticles and the effect on its chaperone activity was evaluated using three model substrate proteins. When CS was used as a substrate protein, B1NTR-NPs (10 nm) exhibited a dose-dependent suppression of heat-induced CS aggregation, with no effect on the

lag phase (Figure 26A). Similar dose-dependent suppression was obtained when MDH was the substrate (Figure 26B). However, in contrast to the results with CS, even very low concentrations of B1NTR-NP (7.5 nM) exhibited chaperone activity for MDH. B1NTR-AuNPs also slightly increased the lag phase of MDH aggregation. This evidence suggests that conjugation of B1NTR to the AuNPs reduces its mobility, preventing early interactions with some of the denaturing substrates. It is also important to note that, since coupling could occur between the PEG linker and any available terminal amine on B1NTR, it's likely that multiple orientations of the peptide are presented on the NP surface, which may contribute to differences in binding results.

The solubility of B1NTR-AuNP complexes with its substrates, CS and MDH, was analyzed with SDS-PAGE (Figure 26C,D). Increasing concentrations of B1NTR-NP produced slight decreases in the amount of insoluble substrate for both CS and MDH. Although the heterogeneous and insoluble nature of B1NTR-NPs can create smearing of the visible bands, an increase in soluble MDH was observed that correlated with an increase in chaperone activity at higher concentration ratios of B1NTR-AuNPs to MDH. The ability of B1NTR-AuNPs to increase the proportion of soluble MDH was confirmed with TEM imaging.

When methyl-terminated PEG-NPs were mixed with CS, a reduction in aggregation was observed, suggesting possible formation of non-specific

interactions between the PEG-NP and denaturing CS. This phenomenon could also be explained by a failure of the PEG linker to thoroughly coat the AuNP, leading to possible substrate-AuNP surface interactions. When PEG-NPs were mixed with MDH, an opposing result was obtained. An increase in MDH aggregation indicated that the PEG-NPs do not contribute to the suppression of MDH aggregation by B1NTR-NPs. These results do suggest interactions between the substrate, MDH, and PEG-NPs, but not in a favorable, chaperone-like manner. Because this interaction is different from the interaction between CS and PEG-NPs, the hypothesis that PEG-NPs interact non-specifically with substrates proteins is supported. Further examination of these non-specific interactions may provide knowledge regarding interactions between denatured proteins and the surface of conjugated nanoparticles.

It is evident that conjugating B1NTR to PEG-NPs retains its chaperone activity and does not impede the binding of substrates, a necessary feature of potential sHsp mimics. Additionally, results from using both unconjugated and conjugated B1NTR consistently suggest that the chaperone activity attributed to B1NTR is more effective for MDH than CS. Since both are heat-denatured substrates, this suggests that chaperone behavior is influenced by factors beyond a substrate's mode of denaturation.

To study the effect of substrate denaturation conditions on the chaperone-activity of B1NTR-AuNPs, the experiments described above were

repeated with the DTT-denatured substrate protein Lys. Results indicated a decrease in the lag phase, as well as an increase in overall substrate aggregation in the presence of more concentrated B1NTR-AuNP samples (Figure 27B). Little chaperone activity was observed for more dilute B1NTR-AuNP samples. While free B1NTR exhibited significant chaperone activity for Lys, this data suggests that 10 nm B1NTR-AuNPs may facilitate, rather than reduce, Lys aggregation. However, when 5 nm B1NTR-NPs were evaluated under the same conditions, a concentration-dependent decrease in aggregation was observed, along with an increase in the lag phase (Figure 27C). These results indicate interactions between B1NTR-AuNPs and Lys differ depending on the diameter of the nanoparticle.

4.5 | Chaperone Activity of CryAAID1-Conjugated Nanoparticles

Many differences were observed between the chaperone activity of the entire NTR of human sHsp HspB1 and CryAAID1 (an 18 residue peptide from the NTR of alpha-crystallin A). These studies facilitate our binding site mapping within the NTR of sHsps and identify protein sequences that contribute to transient protein-protein interactions.

To characterize the *in vitro* chaperone activity of CryAAID1 (residues 70-88 of alpha-crystallin A), its capability to suppress the DTT-induced aggregation of Lys was evaluated (Figure 28A). The more concentrated sample of soluble CryAAID1 displayed an increase in the lag phase, while the less

concentrated sample did not. However, the more dilute sample of CryAAID1 displayed greater overall chaperone activity for Lys. This may be due to the mechanism of aggregation under dilute chaperone conditions. The increase in the lag phase for the more concentrated sample suggests the CryAAID1 peptide may interact with the substrate early in the unfolding process to prevent aggregation, and is able to maintain chaperone activity to some extent over time. At lower concentrations, CryAAID1 does not alter the lag phase (start of aggregation), perhaps due to less available chaperone in solution, but overall is able to suppress aggregation to a greater extent. This difference may be attributed to differences in oligomeric formations and availability of substrate-binding based on sHsp concentration. Perhaps peptide-peptide interactions are occurring in solution between the chaperones that lessen their activity at high concentrations.

When conjugated to 10 nm AuNPs, CryAAID1 displayed significant chaperone activity at higher concentrations. These results suggest the immobilization of the peptide on the surface of AuNPs prevents interactions that may have been happening with free peptide in solution that cause a weakening of chaperone activity. Once conjugated to 5 nm AuNPs, CryAAID1 exhibited less chaperone activity for Lys and did not alter substrate aggregation until present at extremely high concentrations (Figure 29). Perhaps the smaller NP diameter allowed peptide-peptide interactions while conjugated to the surface that prevented substrate-binding from taking place.

When evaluating CryAAID1 substrate specificity and chaperone activity for Ins, the peptide displayed significantly higher aggregation suppression when compared to Lys. Conjugated to 10 nm AuNPs, CryAAID1 displayed dose-dependent suppression of Ins aggregation (Figure 30). It's likely that interactions between CryAAID1 and Ins are of a different nature than those between CryAAID1 and Lys, allowing for more efficient chaperone activity. However, like with Lys, 5 nm CryAAID1-AuNPs displayed little to no chaperone activity (Figure 31). These results further suggest that the size of the NP has a large effect on the peptide's chaperone ability, and that smaller NP diameters are less favorable for facilitating substrate binding.

Finally, a third model substrate, alpha-Lac, was used to characterize the activity of CryAAID1-AuNPs. Chaperone activity of the free peptide on alpha-Lac was mid-range in comparison to Lys and Ins, supporting the hypothesis that CryAAID-substrate binding is substrate specific. 10 nm CryAAID1-AuNPs displayed similar chaperone activity at all concentrations with no dose-dependent trend, suggesting conjugation altered CryAAID1 activity (Figure 32). Consistent with the other substrates tested, 5 nm CryAAID1-AuNPs did not display significant overall chaperone activity for alpha-Lac. However, the 5 nm CryAAID1-AuNPs did appear to eliminate the presence of an intermediate in the unfolding of alpha-Lac (Figure 33). These results are preliminary, and repetitions

must be performed to confirm (5 nm) CryAAID1-AuNP-dependent presence and absence of alpha-Lac unfolding intermediate.

In summary, when CryAAID1 was conjugated to 10 nm AuNPs, some concentration-dependent chaperone activity was observed for several substrates. In general, little to no chaperone activity was observed when the peptide was conjugated to 5 nm AuNPs, suggesting the observed chaperone activity is highly dependent on the surface characteristics and properties of the conjugated nanoparticles and that multivalency effects can be modified or tuned by modifying the nanoparticle structures.

4.6 | Conclusions and Future Directions

These results demonstrate the *in vitro* chaperone activity of the NTR of a human sHsp, HspB1, in the absence of the highly structured ACD and the CTR. Additionally, the B1NTR exhibits substrate specificity when comparing activity for three model substrates. While these results likely do not represent all of the physiological interactions of wild-type sHsps, this study presents difficult-to-characterize evidence that sHsp NTRs directly interact with substrates and impart chaperone activity under varying conditions and concentrations. Additionally, this study shows that NP probes have the ability to increase the chaperone capacity of B1NTR *in vitro*. These B1NTR conjugated AuNPs provide a new approach to exploring the relationship between the sHsp and its unfolded substrate. Conjugated gold nanoparticle studies enable the investigation of the

role of protein quaternary structure and multivalency in chaperone activity, since NTR-conjugated AuNPs simulate the function of sHsp oligomers while lacking the dynamic features of full-length sHsps. Results suggest that both substrate binding and oligomerization of sHsps contribute to chaperone activity, perhaps by modulating the availability of binding sites. This modulation, as well substrate binding itself, has been shown in this work to require the NTR of the sHsp. Increases in chaperone capacity are made possible when the NTR is involved only in substrate binding and not in sHsp oligomerization. However, for some substrates like CS, the NTR has been shown not to be the only region of the sHsp involved in chaperone activity, as demonstrated by the decrease in chaperone capacity for CS by B1NTR compared to full-length HspB1.

A powerful method to bioengineer potent peptide therapeutics is to fuse peptides to nanoparticles, which provides a platform for controlled molecular weight, cellular release, assembly, and multivalency.[1] The results presented here suggest peptide-conjugated nanoparticles may act as tunable chemical probes to examine the importance of multivalent interactions, protein dynamics, and protein-protein interactions that underlie non-enzymatic chaperone activity, allowing for the investigation of sHsp function within the chaperone network. In pathology treatments, the surface characteristics of the NPs could be tuned to possibly select for target cellular substrates.

In studying CryAAID1-AuNPs, results suggest the size of NPs has an impact on the conjugate's chaperone activity and confirm that like B1NTR, the CryAAID1 peptide retains chaperone activity in the absence of the rest of the sHsp and also displays substrate specificity.

In the future, additional work is needed to identify the specific amino acids and post-translational modifications that comprise sHsp-substrate interacting domains for different substrates. Future experiments should also seek to answer whether denaturing substrates interact with multiple sites on sHsps. Furthermore, do different substrates interact with different combinations of sites on sHsps? The McMenimen lab is planning to continue characterization of several sHsps, including alpha-crystallin A and alpha-crystallin B, through work with conjugated Au-NPs and point mutation experiments, as well as work to increase the number of substrates for which sHsp chaperone-like activity has been evaluated.

Chapter 4 References

1. Gliniewicz, E. F.; Chambers, K. M.; De Leon, E. R.; Sibai, D.; Campbell, H. C.; McMenimen, K. A. Chaperone‐like activity of the N‐terminal region of a human small heat shock protein and chaperone‐functionalized nanoparticles. *Proteins: Structure, Function, and Bioinformatics* **2019**.

SUPPLEMENTAL INFORMATION

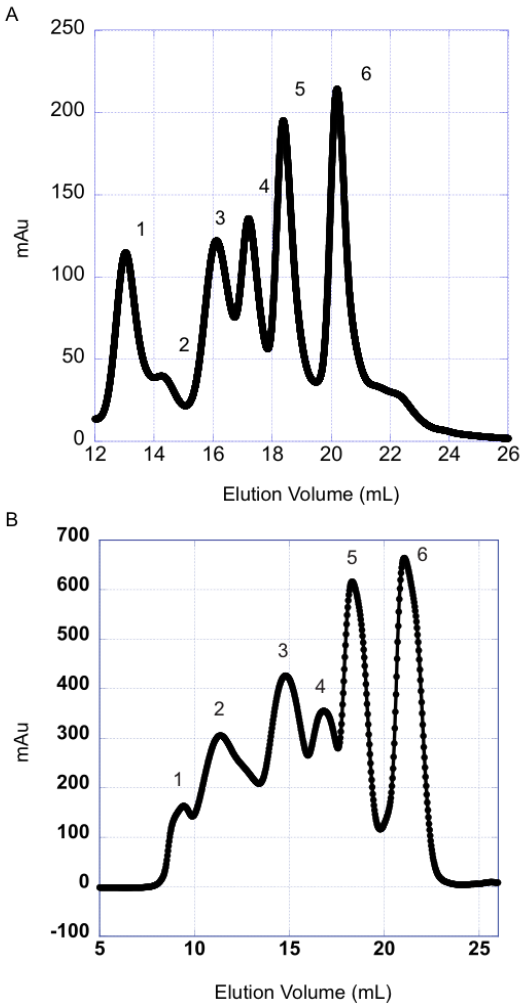

Figure S1. A) Size exclusion chromatography standards. Size exclusion chromatography of molecular weight standards eluted (0.3 mL/min.) from a Superose 6 increase 10/300 column attached to an AKTA FPLC for calibration. The peaks are assigned as follows: 1. aggregate peaks (>670kD), 2. thyroglobulin (669 kDa), 3. g-globulin (158 kDa), 4. ovalbumin (44 kDa), 5. myoglobin (17 kDa), 6. vitamin B_{12} (1.35 kDa). **B)** Size exclusion chromatography standards. Size exclusion chromatography of molecular weight standards eluted (0.3 mL/min.) from a Superdex 200 10/300 column attached to an AKTA FPLC for calibration. The peaks are assigned as follows: 1. aggregate peaks (>670kD), 2. thyroglobulin (669 kDa), 3. g-globulin (158 kDa), 4. ovalbumin (44 kDa), 5. myoglobin (17 kDa), 6. vitamin B_{12} (1.35 kDa).

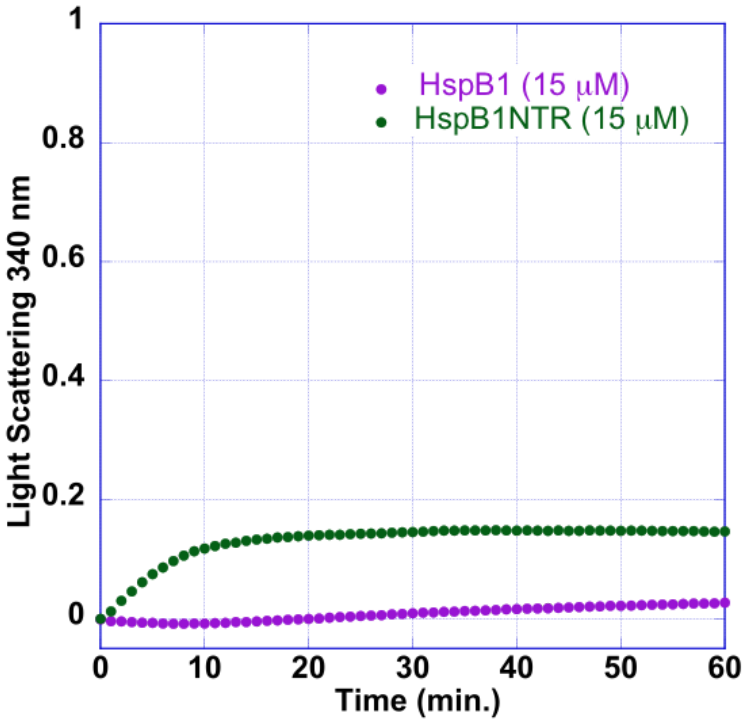

Figure S2. Wild type HspB1 and unconjugated B1NTR heat stability. Heat stability of HspB1NTR and HspB1. (A) No aggregation of HspB1 (15 mM) HspB1 or B1NTR (15 mM) is observed at 45°C. Each curve is an average of ≥ 5 replicates.

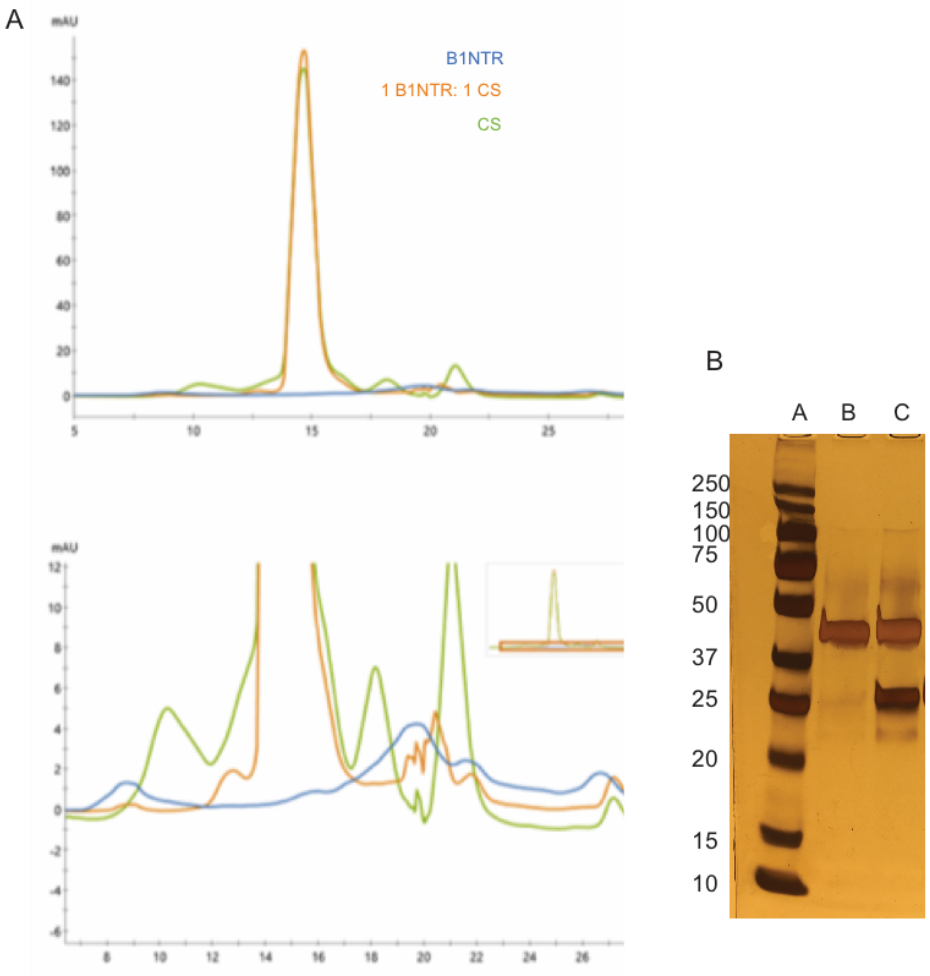

Figure S3. CS and B1NTR (1:1) complexes observed by SEC and SDS-PAGE. (A) SEC profiles of B1NTR, blue curve (7.5 mM), B1NTR (7 mM) + CS (7 mM) orange curve, or CS, green curve (7 mM) only. **(B)** SDS-PAGE analysis of major peaks eluted during SEC analysis. The molecular mass marker (A), CS only major peak (B), and CS + B1NTR mixture major peak are presented in each respective lane. All of these curves were obtained on a Superdex 200 10/30 column.

Table S1. Characterization of size, surface features, diameter (from DLS measurements), zeta potential, and approximation of peptides/particle at 25°C.

Particle	Peptide	Linker/Surface	DLS Size (nm)	Zeta potential (mV)	~ Peptides/particle
10 nm AuNP	none	citrate	16	-35	n/a
10 nm AuNP	none	PEG-CH3	n.d.	-4	n/a
10 nm AuNP	none	PEG-NHS	41	n.d.	n/a
10 nm AuNP	HspB1NTR	PEG	37	-6	> 10
10 nm AuNP	mini-αA	PEG	31	-6	> 100

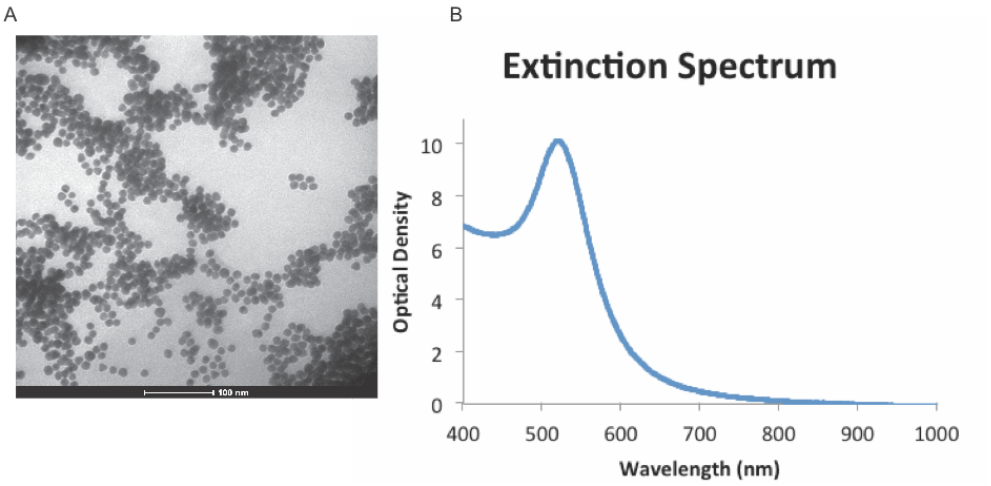

Figure S4. Description of conjugated nanoparticle species. (A) Transmission electron microscopy of HspB1NTR-AuNP in 1x PBS with 0.05% Tween 20. **(B)** Extinction spectrum measuring optical density with λ_{ODmax} = 521 nm. HspB1NTR-NPs are estimated to contain ≥10 HspB1NTR conjugates per particle. Characterization of nanoparticles was performed by Nano Hybrids, Inc (Austin, TX).

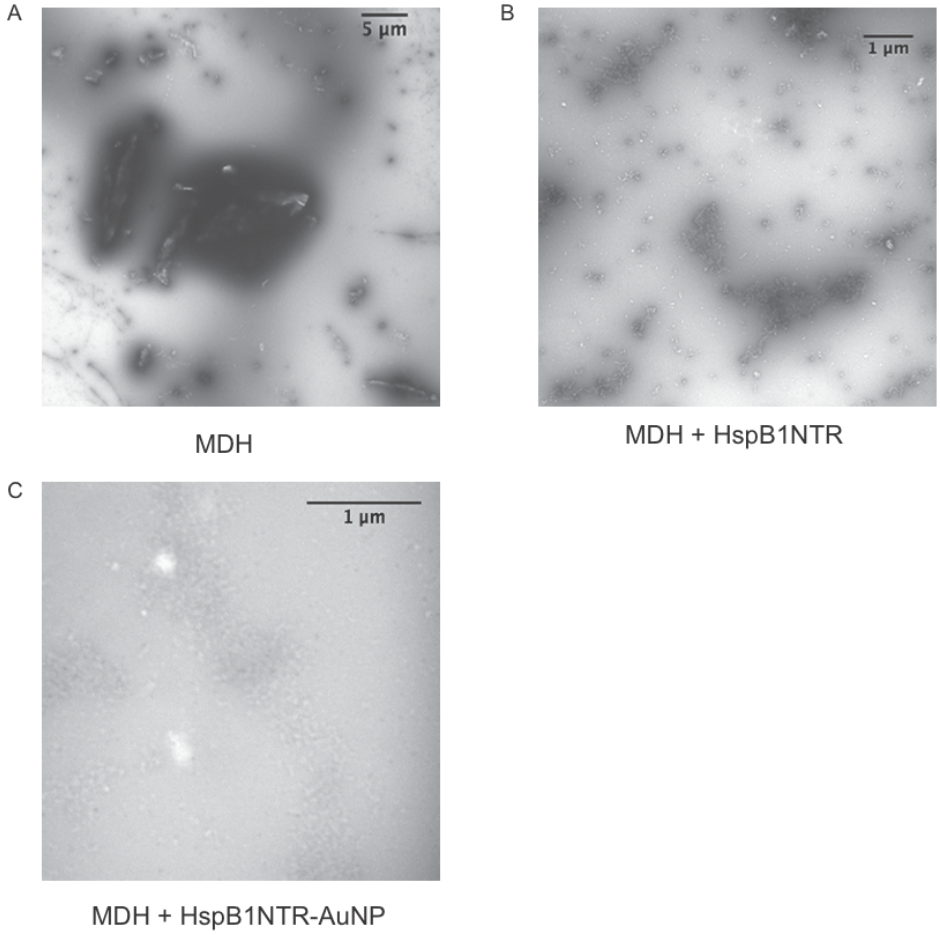

Figure S5. Transmission electron microscopy of MDH in the presence of conjugated and unconjugated HspB1NTR. The presence of HspB1NTR and HspB1NTR-NP changes the physical properties of the substrate, MDH. Figure shows transmission electron microscopy (TEM) images of the MDH in the presence and absence of HspB1NTR. The protein mixtures MDH (2.5 µM), MDH (2.5 µM) + B1NTR (15 µM), and MDH (2.5 µM) + B1NTR-NP (OD2) were prepared in 1x PBS (pH 7.4) and heated at 45ºC for 1 hr with constant stirring. After 1 hr, 4 µL of each sample was applied to a carbon-coated 150 mesh copper grid (Electron Microscopy Sciences, Hatfield, PA) at room temperature, stained with freshly prepared 4% uranyl acetate, and examined under a Phillips/FEI CM100 (100kV). The images were obtained using an AMT digital camera and analyzed with ImageJ. **(A)** MDH (2.5 µM) after incubation at 45°C for 40 min, magnification 1450x. **(B)** MDH (2.5 µM) + B1NTR (2.5 µM) heated at 45°C for 40 min, magnification 5800x. **(C)** MDH (2.5 µM) + B1NTR-NP (14.9 nM) heated at 45°C for 40 min, magnification, 19000x. Figure from Gliniewicz *et al*., 2019.

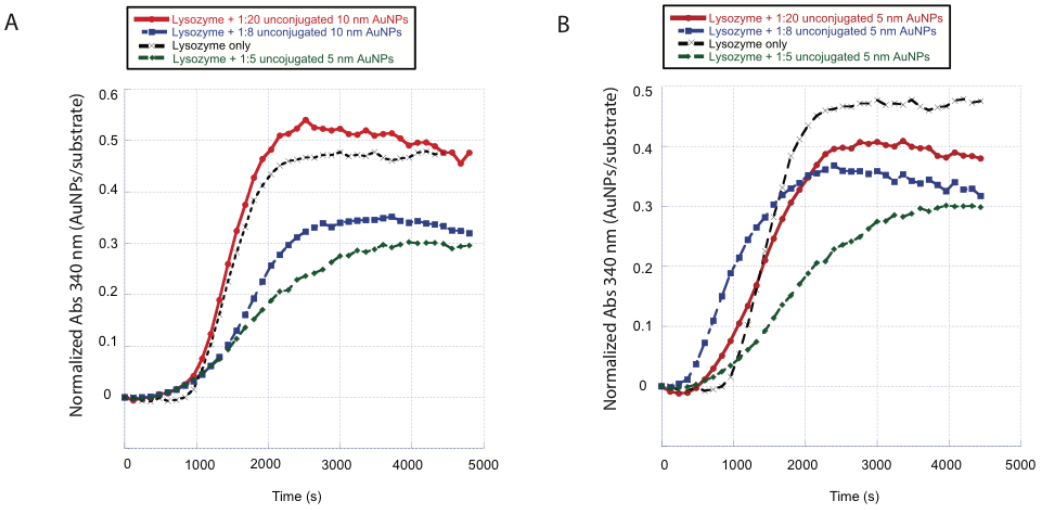

Figure S6. Aggregation of lysozyme with unconjugated 5 & 10 nm citrate-capped AuNPs. (A) Concentration-dependent aggregation of lysozyme (35mM) with 10 nm citrate-capped AuNPs (OD 1 initial concentration) diluted to 1:5 (green), 1:8 (blue), and 1:20 (red). As concentration of unconjugated citrate AuNPs is increased, a corresponding decrease in Lys aggregation is observed. **(B)** Aggregation of Lys (35 mM) is not concentration-dependent in the presence of 5 nm citrate-capped AuNPs (OD 1 initial concentration) diluted to 1:5 (green), 1:8 (blue), and 1:20 (red). Data was normalized to the maximum absorbance of the averaged Lys curves. Each curve is the average of ³ 3 independent trials.